Finite Elements in Analysis and Design 119 (2016) 15–29

Contents lists available at ScienceDirect

Finite Elements in Analysis and Design

journal homepage: www.elsevier.com/locate/finel

Full Length Articles

A reduced basis approach for the parametric low frequency response of submerged viscoelastic structures

C. Leblond *, J.-F. Sigrist

DCNS Research, Département Dynamique des Structures, 5 rue de l'Halbrane, 44340 Bouguenais, France

ARTICLE INFO

Article history:
Received 1 September 2015
Received in revised form
23 March 2016
Accepted 16 May 2016
Available online 3 June 2016

Keywords:
Structure–acoustic interaction
Viscoelasticity
Finite element method
Reduced order model
Reduced basis
Greedy algorithm

ABSTRACT

Reduced Order Models (ROMs) are proposed to compute the frequency response of submerged viscoelastic structures with variation of parameters. A parameterized matrix system is first derived from the finite element discretization of a structural-acoustic formulation, to constitute both the full model of reference and the starting point of the ROMs building. The low dimensional trial subspace is obtained offline with an iterative greedy algorithm inspired by the Reduced Basis method. Galerkin and Minimum Residual projections are then considered to determine the test subspace and construct the parametric online-efficient ROMs. Their accuracy and robustness are evaluated on two test cases: a submerged composite viscoelastic plate and a submerged propeller with viscoelastic patches. They are moreover compared to established methods conceived to tackle in vacuo viscoelastic problems, and extended here for submerged structures. Convergence properties as functions of the decomposition order are computed and discussed on parameter spaces of dimensions one and four. The resulting CPU time gain compared to full model evaluations opens the way to efficient design strategies, taking into account the parameters variabilities.

1. Introduction

The computation of submerged structures responses to weak forced mechanical solicitations remains a CPU time-consuming process in naval industry, on account on the large size of the underlying problems, their geometrical complexities, as well as the strong coupling with the fluid. The finite element discretization of such a forced vibration problem usually results in a linear matrix system with millions of degrees of freedom, which has to be inverted at each frequency of interest. In practice, analyzes on very coarse frequency grids are performed in order to reduce the overall time of the computation. In the design process of vessels or submarines, the choice of the materials and their characteristics, if known, may moreover evolve, so that numerous computations are theoretically required with new values of the parameters. Once again, the large CPU-time requirement drastically limits the number of shots performed in practice, which may ultimately affect the robustness and optimality of the design.

In order to reduce both the structural vibrations and the noise radiation, viscoelastic damping technologies are receiving a growing interest in naval industry. The use of such highly dissipative materials nevertheless complicates the numerical modeling and computation of the problem. For instance, the stiffness matrix resulting from the finite element discretization becomes complex-valued and frequency-dependent. Furthermore, viscoelastic materials are very sensitive to non-mastered operational conditions, for example the temperature, and their constitutive mathematical model are rarely fully determined. A robust design should take into account these uncertainties, increasing the dimension of the parameter space to consider.

Model reduction techniques are developed and evaluated in this paper, so as to make tractable analyzes on very fine frequency grids, as well as to handle the complexity of a relatively high-dimensional parameter space, for viscoelastic and submerged structures. Reduced Order Models (ROMs) are nowadays able to represent complex systems with few degrees of freedom at the cost of a moderate loss of accuracy. Numerous techniques can be found in the literature to build a ROM. Most of them involve the knowledge of a low-dimensional basis as starting point, such as Proper Orthogonal Decomposition [1], balanced Proper Orthogonal Decomposition [2], A Priori Reduction [3,4], Proper Generalized Decomposition [5–9] and Reduced Basis [10,11], just to name a few. The crucial point to obtain a reliable parametric ROM is to build a reduced trial space that spans most of the physics at hand, over the whole parameter space of interest. Obviously, the reduced basis has to be of much lower dimension than the discretized full model, for a real-time (or at least very fast) online evaluation of the ROM solution.

* Corresponding author. Tel.: +33 2 44 76 57 93.
E-mail address: cedric.leblond@dcnsgroup.com (C. Leblond).

http://dx.doi.org/10.1016/j.finel.2016.05.002
0168-874X/

In the case of a one-dimensional parameter space, involving only the frequency ω, established reduction methods can be found in the literature to tackle part of the problem of interest (a submerged viscoelastic structure):

- For linear problems involving *in vacuo* elastic structures, the classical modal basis remains the most appropriate basis for reduction. The real-valued eigenvectors are computed through highly efficient and powerful algorithms, even for very large sparse symmetrical real-valued mass and stiffness matrices. The Proper Orthogonal Decomposition and A Priori Reduction have also been evaluated with success for the reduction of such linear (and nonlinear) structural dynamics problems [12,13].
- For *in vacuo* viscoelastic structures, the discretized full model equation can take the form $\left[-\omega^2\mathbf{M}+\mathbf{K}(\omega)\right]\mathbf{X}(\omega)=\mathbf{B}(\omega)$, with the symmetrical real-valued matrix $\mathbf{M}$ and the symmetrical complex-valued and frequency-dependent matrix $\mathbf{K}(\omega)$. The corresponding eigenvalue problem, $\left[-\omega^2\mathbf{M}+\mathbf{K}(\omega)\right]\Psi=0$, appears to be non-trivial due to its non-linearity. The Modal Strain Energy (MSE) approach [14] consists in neglecting the frequency dependence of the stiffness matrix to obtain the eigenvectors: they are therefore solutions of the eigenvalue problem $\left[-\omega^2\mathbf{M}+\mathbf{K}(\omega_0)\right]\Psi=0$, with ω_0 being the minimum frequency of interest for instance. To reduce the computational time of the basis calculation and work only with real-valued modes, a widespread practice consists in keeping only the real part of the stiffness matrix when solving this eigenvalue problem. These approaches, easy to implement and cost-effective, are of course limited to weakly damped materials or to a close vicinity of ω_0. For highly damped structures, more expensive and accurate methods are available. For instance with the Iterative Modal Strain Energy (IMSE) approach [15], each mode is computed through an iterative algorithm, in which the real part of the stiffness matrix is updated in the eigenvalue problem $\left[-(\omega^{(i)})^2\mathbf{M}+Re\{\mathbf{K}(\omega_m^{(i-1)})\}\right]\Psi^{(i)}=0$. The Iterative Complex Eigensolution (ICE) approach [16,17] follows the same iterative strategy, while keeping the whole complex stiffness matrix. It is therefore more physically consistent for highly damped structures, but also more time-consuming due to less powerful algorithms available to solve large complex eigenvalue problems. Another strategy consists in computing several bases, solutions of the eigenvalue problems $[-\omega^2\mathbf{M}+\mathbf{K}(\omega_j)]\Psi=0$ for $j=1\ldots J$, and in assembling them with a Gram–Schmidt process. The choice of the values of ω_j is performed *ad hoc*, guided by the physics of the problem. This multi-model approach has been successfully evaluated on highly damped structures [18,19]. An alternative family of strategies, applied on problems involving viscoelasticity and nonlinear behavior [20], considers the frequency as an extra-coordinate. This approach based on Proper Generalized Decomposition leads to efficient and accurate harmonic analysis [21,22]. It has been successfully applied on several test cases, involving relatively light full scale models.
- For elastic and weakly viscoelastic structures submerged in a finite fluid domain, the available methods are mostly based on a dynamic substructuring procedure [23], involving the acoustic modes and the zero-frequency static solutions in the fluid part, as well as the undamped and uncoupled structural modes. These potentially efficient reduction approaches require a development effort to be industrially usable, since they are not based on a precomputed monolithic structural-acoustic full model. Another strategy consists in using the boundary elements method to account for the infinite fluid domain effect [24], through a frequency-dependent additional mass matrix in the structural finite element matrix system. The reduction may then be achieved via a Galerkin projection onto the in vacuo undamped structural modes [24–27].

This review, although not comprehensive, suggests that the literature on the space-frequency reduction of problems involving submerged viscoelastic structures is rather scarce: their accuracies may be guaranteed for weakly damped structures, but the question of robustness of the reduced trial basis remains open for highly damped materials. The most suitable and available methods for industrial use still involve *ad hoc* and non-automatic procedures, at the risk of inaccurate estimations of the quantities of interest.

The multidimensional character of the parameter space constitutes here an additional challenge. This aspect does not appear to be specifically tackled in the field of structure–acoustic interaction problems, despite underlying industrial needs. Several techniques are of course emerging in other domains to treat such parametric studies. Among them, a line of research focuses on the interpolation of precomputed bases, to yield a space basis adapted to a new parameters values. More precisely, the subspace angle interpolation [28], as well as an advanced interpolation based on the Grassmann manifold and its tangent space [29], are developed and successfully tested in the field of aeroelasticity. Since these approaches are essentially geometrical and do not take into account the underlying equations, the precomputed bases still require to be close enough to the new parameters values to yield an accurate ROM. The Proper Generalized Decomposition (PGD) constitutes another serious candidate, with numerous successful applications on multidimensional parametric models [30–32]. More precisely, the family of strategies considering the frequency as an extra-coordinate has also been developed and evaluated in the parametric framework [21,22]. It is shown that, with the increase of dimensionality, the internal fixed point algorithm requires more iterations to converge and that the PGD expansion requires a higher rank to reach a given accuracy. The overall number of calls to the full scale model is nevertheless reasonable, which enables us to decrease by several orders of magnitude the CPU time compared to a brute force approach sampling. The application of a PGD-like approach for the computation of the submerged structures responses with uncertain parameters is indeed a work in progress [33,34]. We address in the present study the challenge of sampling a relatively high-dimensional parameter space to iteratively build an appropriate trial basis, by following the framework of the Reduced Basis method along with the use of a greedy algorithm [10,11,35,36]. Contrary to PGD algorithms, there is no fixed point algorithm to compute each new term of the expansion; the overall number of calls to the full scale model is therefore expected to be very small, which is of paramount importance for industrial applications.

The goal is here to obtain a parametric ROM, suitable for real-time online use and accurate when the parameters vary. The offline computation of the reduced basis may be CPU time-consuming, but it has to be of the same order of a standard industrial study: in other words, it should be feasible on a workstation for scientific computation in a design office. Another constraint of the study lies on the weakly intrusiveness of the reduction method: the fluid–structure full scale model, on which the reduced model is built, does not have to be fully considered as a black-box, but the effort of implementation within it has to remain limited. More precisely, the approach is conceived to be usable within a standard industrial FEM software, by definition less opened than a homemade dedicated numerical code. The resulting reduction strategy proposed here follows this guideline.

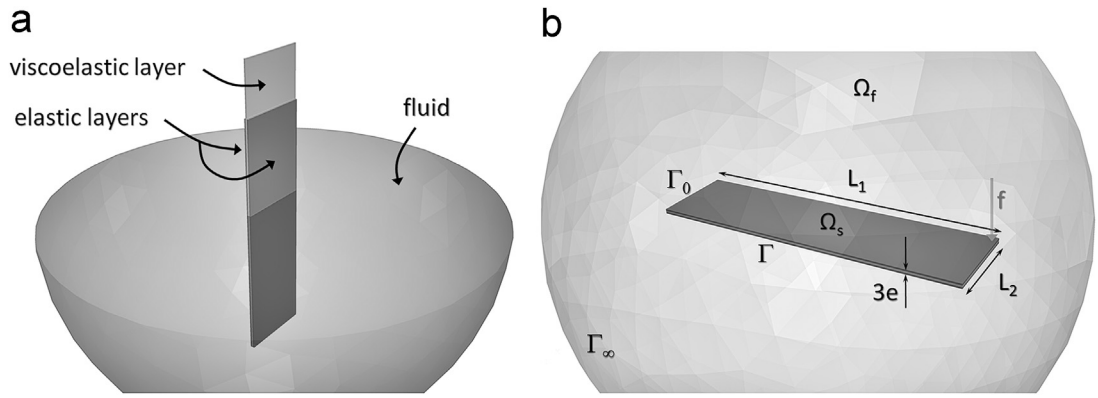

Fig. 1. Submerged composite plate with a viscoelastic layer; (a) slices of the studied geometry, (b) mesh and notations.

Table 1
The variables are normalized by the fluid density $\tilde{\rho}_f$, the speed of sound in the fluid $\tilde{c}_f$ and a characteristic length $\tilde{L}$. The values $\tilde{\rho}_f = 1000$ kg m^{-3}, $\tilde{c}_f = 1500$ m s^{-1} and $\tilde{L} = 1$ m are used for the cases illustrated in the present paper.

Variable	Normalization factor
Length, displacement	$\tilde{L}$
Time	$\tilde{L}/\tilde{c}_f$
Frequency	$\tilde{c}_f/\tilde{L}$
Density	$\tilde{\rho}_f$
Pressure, stress	$\tilde{\rho}_f\tilde{c}_f^2$
Potential	$\tilde{L}^2$
Impedance	$\tilde{\rho}_f\tilde{c}_f$

The different steps of the approach are not new in themselves. The main contribution of the present work lies in a careful choice and assembly of each step of the algorithm, so as to constitute a reduction method able to tackle cases of industrial complexity. This is subjectively not so common in the reduced order model community.

The full model of interest is described in Section 2. A symmetrical formulation suitable for very large-scale structure–acoustic interaction problems is recalled and turned into a parameterized matrix system via finite element discretization. This matrix system constitutes the starting point of the reduced-order modeling in Section 3. The proposed methodology, based on a discretized version of the structure–acoustic interaction problem, is motivated by the intention to construct the reduced models with the same numerical operators as those used for the full model. This should avoid discretization discrepancies between the full and reduced models, and should limit the intrusiveness and effort of implementation. For the building of the ROMs, Galerkin and minimum residual projections are considered in Section 3.2 and the greedy algorithm to construct the reduced basis is explicitly formulated in Section 3.3 for a multidimensional parameter space. The reduced models are then illustrated on two test cases in Section 4. The first one, Section 4.1, involves a submerged simple composite plate with a viscoelastic layer. It enables us to compare the proposed ROMs with existing approaches, when only the frequency varies. Then a four-dimensional parameter space is considered and the accuracy of the ROMs is evaluated by comparison with several full model evaluations. The ROMs are then applied on an industrial case in Section 4.2, consisting of a submerged propeller with embedded viscoelastic patches. Some improvements and extensions of the proposed method are finally suggested in the conclusion.

2. Full model

2.1. Strong formulation

A body submerged in a fluid domain $\tilde{\Omega}_f$ is considered in the present paper, see for instance Figs. 1(b) and 9(b). The tildes are used in the following to denote dimensional quantities. Conversely, no tilde will imply a non-dimensional quantity, normalized according to Table 1. The body, defined by the domain $\tilde{\Omega}_s$ of boundary $\partial\tilde{\Omega}_s$, can be made of different materials with both elastic and viscoelastic constitutive laws. The fluid medium is assumed at rest with an acoustic behavior and interacts with the body on the boundary $\tilde{\Gamma} \in \partial\tilde{\Omega}_s$. Numerous formulations can be found in the literature to model the structure–acoustic interaction problem. We choose here the symmetrical (displacement, pressure, potential) formulation [37,38] since it is available in many finite element industrial softwares, and is proven to be efficient for tackling very large-scale problems. The whole methodology proposed in the present paper can nevertheless be straightforwardly applied to other formulations.

For the structural dynamics, the non-dimensional governing equations are classically given in the frequency domain by:

$$\begin{aligned} &-\omega^2\rho_s\,\mathbf{u} - \nabla\cdot\sigma(\mathbf{u}) = \mathbf{0} \quad \text{in } \Omega_s \\ &\sigma(\mathbf{u})\cdot\mathbf{n}_s = \mathbf{f} \quad \text{on } \Gamma_s \\ &\sigma(\mathbf{u})\cdot\mathbf{n}_s = \omega^2\phi\mathbf{n} \quad \text{on } \Gamma \\ &\mathbf{u} = \mathbf{0} \quad \text{on } \Gamma_0 \end{aligned} \tag{1}$$

with $\mathbf{u}$ being the structural displacement field and ϕ the displacement potential. Moreover, ω denotes the frequency, ρ_s the density of the structure, $\mathbf{n}_s$ and $\mathbf{n}$ the outward unit normals of the body and the fluid domains, respectively. $\mathbf{f}$ is a mechanical forcing term acting on the body boundary $\Gamma_s \in \partial\Omega_s$. Linear isotropic viscoelastic models are considered for the structure so that the stress tensor σ can be written under the form $\sigma(\mathbf{u}) = E(\omega)\mathbf{K}^0 : \varepsilon(\mathbf{u})$, with $E(\omega)$ being the complex frequency dependent Young modulus and ε the symmetric strain tensor. $\mathbf{K}^0$ denotes the Hooke elasticity tensor associated to a unitary Young modulus.

The non-dimensional governing equations for the acoustical fluid medium, in terms of pressure p and displacement potential ϕ, can be written as [37,38]:

$$\begin{aligned} &p - \omega^2\phi = 0 \quad \text{in } \Omega_f \\ &\nabla^2\phi + p = 0 \quad \text{in } \Omega_f \\ &\nabla\phi\cdot\mathbf{n} = \mathbf{u}\cdot\mathbf{n} \quad \text{on } \Gamma \\ &\nabla\phi\cdot\mathbf{n} = -i\omega\,\frac{\phi}{Z(\omega)} \quad \text{on } \Gamma_\infty \end{aligned} \tag{2}$$

Only the displacement $\mathbf{u}$ and the pressure p have a physical meaning. The displacement potential ϕ is an auxiliary variable

introduced in order to obtain a symmetrical structure–acoustic formulation ($\mathbf{u}$, p, ϕ). Note that the first two equations of (2) lead to the classical non-dimensional wave equation for the fluid pressure. In the last relation of (2), $Z(\omega)$ denotes a complex valued impedance to apply on a boundary Γ_∞. More precisely, this boundary condition is introduced in order to account for the condition of non-reflexion of acoustic waves at the truncated fluid domain. Various approximations of such condition can be found in the literature. In the present case, the impedance $Z(\omega)=1/(1+\tilde{L}/(i\omega\tilde{R}_\infty))$ is applied on the spherical surface Γ_∞ of radius $\tilde{R}_\infty$. This choice, corresponding to the BGT condition of order 1 [39,40], is motivated not only for its enhanced accuracy compared to the BGT condition of order 0, $Z=1$, but also for its ease of implementation within a finite element numerical software [41].

As a remark, the resulting dimensionless $(\mathbf{u},p,\phi)$ formulation, Eqs. (1) and (2), is singular for $\omega=0$. This does not constitute a specific issue for the reduced order method and cases of concerned here, but the singularity should be removed if rigid body motions are of interest [23].

2.2. Variability of the system parameters

The main goal of the present paper is to obtain a parametric ROM, *i.e.* a ROM able to evaluate in real time structural and acoustical quantities when the system parameters vary. The nature of these variations may be either deterministic, induced by new values inside an iterative optimization algorithm for instance, or random, modeling materials uncertainties. The parameters set $\mathcal{D}\subset\mathbb{R}^P$ is now defined and a point in this set is denoted $\mu\equiv\{\mu_1,\ldots,\mu_P\}$. The variations of the physical parameters are considered through the parameterized quantities $\omega(\mu)$, $\rho_s(\mu)$ and $E(\mu)\equiv E(\omega(\mu),\mu)$. In Section 4, illustrations are performed for $P=1$ and $P=4$.

2.3. Weak formulation

The spatial-weak formulation of the structure–acoustic interaction problem (Eqs. (1) and 2) can be easily written within the usual framework of complex Hilbert spaces. By denoting the spaces $\mathcal{U}=\{\mathbf{v}\in(H^1(\Omega_s))^3\,|\,\mathbf{v}=\mathbf{0}\text{ on }\Gamma_0\}$ and $\mathcal{V}=\mathcal{U}\times L^2(\Omega_f)\times H^1(\Omega_f)$, it takes the form: find $X(\mu)=(\mathbf{u}(\mu),p(\mu),\phi(\mu))\in\mathcal{V}$ such that

$$\mathcal{A}(X(\mu),\delta X;\mu)=\mathcal{B}(\delta X),\quad\forall\delta X\in\mathcal{V} \tag{3}$$

with $\mathcal{A}:\mathcal{V}\times\mathcal{V}\times\mathcal{D}\to\mathbb{C}$ a parameterized sesquilinear form and $\mathcal{B}:\mathcal{V}\to\mathbb{C}$ a linear form.

In case of a structure made of L constant properties materials, with $\Omega_s=\cup_{l=1}^{L}\Omega_s^l$ and $\Omega_s^l\cap\Omega_s^k=\varnothing$ for $l\neq k$, we introduce the following quantities for $l=1\ldots L:\rho_s^l(\mu):\mathcal{D}\to\mathbb{R}$ the mass density of the material l and $E^l(\mu):\mathcal{D}\to\mathbb{C}$ its Young modulus. For convenience, we also introduce $\rho_s^0(\mu)=1$ and $E^0(\mu)=1$. The parameterized sesquilinear form $\mathcal{A}:\mathcal{V}\times\mathcal{V}\times\mathcal{D}\to\mathbb{C}$ in Eq. (3) can then be rewritten under an affine form in the parameter:

$$\mathcal{A}(X,Y;\mu)=\sum_{k=0}^{2(L+1)}\lambda^k(\mu)\,\mathcal{A}^k(X,Y),\quad\forall Y\in\mathcal{V} \tag{4}$$

with the complex-valued parameter-dependent coefficients defined by:

$$\begin{aligned}
&\lambda^0(\mu)=-i\omega^3(\mu)/Z(\mu)\\
&\lambda^k(\mu)=-\omega^2(\mu)\rho_s^{k-1}(\mu),\quad k=1\ldots L+1\\
&\lambda^k(\mu)=E^{k-(L+2)}(\mu),\quad k=L+2\ldots 2(L+1)
\end{aligned} \tag{5}$$

As for the sesquilinear forms $\mathcal{A}^k$ and linear form $\mathcal{B}$, they are explicitly given by:

$$\begin{aligned}
&\mathcal{A}^0=-\int_{\Gamma_\infty}\overline{\psi}\phi\,\mathrm{d}\mathbf{x}\\
&\mathcal{A}^1=\int_\Gamma\phi\overline{\mathbf{v}}\cdot\mathbf{n}+\overline{\psi}\mathbf{u}\cdot\mathbf{n}\,\mathrm{d}\mathbf{x}+\int_{\Omega_f}\nabla\overline{\psi}\cdot\nabla\phi+\overline{q}\phi+\overline{\psi}p\,\mathrm{d}\mathbf{x}\\
&\mathcal{A}^k=\int_{\Omega_s^{k-1}}\overline{\mathbf{v}}\cdot\mathbf{u}\,\mathrm{d}\mathbf{x},\quad k=2\ldots L+1\\
&\mathcal{A}^{L+2}=\int_{\Omega_f}\overline{q}p\,\mathrm{d}\mathbf{x}\\
&\mathcal{A}^k=\int_{\Omega_s^{k-(L+2)}}\varepsilon(\overline{\mathbf{v}}):\mathbf{K}^0:\varepsilon(\mathbf{u})\,\mathrm{d}\mathbf{x},\quad k=L+3\ldots 2(L+1)\\
&\mathcal{B}=\int_{\Gamma_s}\overline{\mathbf{v}}\cdot\mathbf{f}\,\mathrm{d}\mathbf{x}
\end{aligned} \tag{6}$$

with $(\mathbf{u},p,\phi)\in\mathcal{V}$ and $(\mathbf{v},q,\psi)\in\mathcal{V}$.

2.4. Finite element model

A finite element approximation space $\mathcal{V}_N\subset\mathcal{V}$ is now introduced: $\mathcal{V}_N=\left\{X^N=\sum_{i=1}^{N}X_i\,\varphi_i\,X_i\in\mathbb{C}\right\}$. The Galerkin approximation $X^N(\mu)\in\mathcal{V}_N$ of $X(\mu)$ is then defined by: find $X^N(\mu)\in\mathcal{V}_N$ such that $\mathcal{A}\left(X^N(\mu),\delta X;\mu\right)=\mathcal{B}(\delta X)$, $\forall\delta X\in\mathcal{V}_N$. This results in the following system of equations for the components $\mathbf{X}(\mu)=\left\{U(\mu),P(\mu),\Phi(\mu)\right\}^T=\left\{X_1(\mu),\ldots,X_N(\mu)\right\}^T\in\mathbb{C}^N$ of the Galerkin approximation $X^N(\mu)$:

$$\delta\mathbf{X}^H\mathbf{A}(\mu)\mathbf{X}(\mu)=\delta\mathbf{X}^H\mathbf{B},\quad\forall\delta\mathbf{X}\in\mathbb{C}^N \tag{7}$$

with $\delta\mathbf{X}^H=\delta\overline{\mathbf{X}}^T$, the conjugate transpose of $\delta\mathbf{X}\in\mathbb{C}^N$. For the structure–acoustic interaction problem considered here and in the case of a structure made of L constant properties materials, the matrix $\mathbf{A}(\mu)\in\mathbb{C}^{N\times N}$ takes the form of a linear combination of parameter-independent matrices:

$$\mathbf{A}(\mu)=\sum_{k=0}^{2(L+1)}\lambda^k(\mu)\,\mathbf{A}^k \tag{8}$$

with the parameter-dependent coefficients defined in Eq. (5), and $\mathbf{A}^k\in\mathbb{R}^{N\times N}$ sparse and symmetric real-valued matrices related to the forms defined in Eq. (6). The parameterized finite element matrix system (7), (8) can now be written as: find $\mathbf{X}(\mu)\in\mathbb{C}^N$ such that

$$\delta\mathbf{X}^H\left[\sum_{k=0}^{2(L+1)}\lambda^k(\mu)\,\mathbf{A}^k\right]\mathbf{X}(\mu)=\delta\mathbf{X}^H\mathbf{B},\quad\forall\delta\mathbf{X}\in\mathbb{C}^N \tag{9}$$

Eq. (9) is numerically convenient since it does not require to rebuild and assemble finite elements matrices as the parameter is varied: the whole finite element symmetric matrix $\mathbf{A}(\mu)$ is simply obtained through linear combination of the precomputed matrices $\mathbf{A}^k$, for $k=0\ldots 2(L+1)$. Note that even if these precomputed matrices are symmetric and real-valued, $\mathbf{A}(\mu)$ is complex-valued and neither Hermitian nor normal. Furthermore $\mathbf{A}(\mu)$ is invertible for $\omega\neq 0$. The discretized finite elements matrix system (7), or in a more explicit form (Eq. (9)), is called *full model* in the following. It constitutes the starting point for the building of the ROMs.

As a remark, some finite element softwares may not provide access to the matrices $\mathbf{A}^k$, but only to the whole matrix $\mathbf{A}(\mu)$ for specified values of the parameter μ. In this case, it is fruitful and straightforward to perform an EIM (Empirical Interpolation Method) [42] on $\mathbf{A}(\mu)$, so as to turn the relation (8) into the less intrusive form:

$$\mathbf{A}(\mu)=\sum_{k=0}^{2(L+1)}\beta^k(\mu)\,\mathbf{A}(\mu^k) \tag{10}$$

with the new functions $\beta^k(\mu)$ and the parameter values μ^k given by the EIM algorithm [36]. This step, very light from the CPU time

point of view, requires only the knowledge of the coefficients $\lambda^k(\mu)$ and access to the sparse matrices $\mathbf{A}(\mu^k)$, for $k=0\ldots2(L+1)$. More details of the algorithm can be found in the work [43]. This differs from the use proposed in [32], in which the discrete EIM enables us to reformulate nonlinear terms in convenient expansions.

3. Reduced order modeling

3.1. Decomposition strategy and error-residual relations

We choose the space-parameter decomposition of order M, for both the structure and fluid variables, under the following monolithic form:

$$\mathbf{X}_M(\mu)=\left\{\begin{array}{c} U_M(\mu) \\ P_M(\mu) \\ \Phi_M(\mu) \end{array}\right\}=\sum_{m=1}^{M}\alpha_m(\mu)\Psi_m=\Psi^M\alpha^M(\mu) \tag{11}$$

with $\alpha_m(\mu)\in\mathbb{C}$ being the parameter functions, $\Psi_m\in\mathbb{C}^N$ the space functions, $\alpha^M(\mu)=\{\alpha_1(\mu),\ldots,\alpha_M(\mu)\}^T\in\mathbb{C}^M$ and $\Psi^M=[\Psi_1,\ldots,\Psi_M]\in\mathbb{C}^{N\times M}$. The number M is of course expected to be small compared to N. This decomposition differs from that used in dynamic substructuring methods, where the fluid and structure variables have their own space bases and generalized coordinates [23]. As it will be shown below, the monolithic form enables us to reduce the intrusiveness of the proposed approach, according to the finite element solver: the building of the ROM requires only access to the precomputed matrices $\mathbf{A}^k$, for $k=0\ldots2(L+1)$, and not to submatrices, as it would be the case with different decompositions for the fields.

Classically, the introduction of the approximate space-parameter decomposition (11) into the discretized full model (7) makes appear a residual $\mathbf{R}_M(\mu)$, explicitly defined by:

$$\delta\mathbf{X}^H\mathbf{R}_M(\mu)=\delta\mathbf{X}^H\big(\mathbf{B}-\mathbf{A}(\mu)\mathbf{X}_M(\mu)\big),\quad\forall\delta\mathbf{X}\in\mathbb{C}^N \tag{12}$$

It is straightforward to show that the error $\mathbf{e}_M(\mu)=\mathbf{X}(\mu)-\mathbf{X}_M(\mu)$ is linked to the residual through the relations:

$$\mathbf{R}_M(\mu)=\mathbf{A}(\mu)\mathbf{e}_M(\mu) \tag{13}$$

$$\mathbf{e}_M(\mu)=\mathbf{A}^{-1}(\mu)\mathbf{R}_M(\mu) \tag{14}$$

where it is assumed that $\mathbf{A}(\mu)$ is invertible. For the following, it is useful to introduce $\|\cdot\|$ the norm associated to the usual scalar product in $\mathbb{C}^N$, $(\mathbf{X},\mathbf{Y})=\mathbf{Y}^H\mathbf{X}$ with $\mathbf{X}$ and $\mathbf{Y}$ in $\mathbb{C}^N$, and $|||\cdot|||$ the related matrix norm defined by $|||\mathbf{A}|||=\sup_{\mathbf{X}\neq0}(\mathbf{AX},\mathbf{AX})/(\mathbf{X},\mathbf{X})$.

3.1.1. Remarks

(i) From (13), it clearly appears that the norm of the residual is equal to the $\mathbf{A}^H\mathbf{A}$–norm of the error: $\|\mathbf{R}_M(\mu)\|^2=\mathbf{e}_M^H(\mu)\mathbf{A}^H(\mu)\mathbf{A}(\mu)\mathbf{e}_M(\mu)=\|\mathbf{e}_M(\mu)\|^2_{\mathbf{A}^H\mathbf{A}}$.

(ii) Eqs. (14) and (7) yield the inequalities $\|\mathbf{e}_M(\mu)\|\leq|||\mathbf{A}^{-1}(\mu)|||\,\|\mathbf{R}_M(\mu)\|$ and $\|\mathbf{B}\|\leq|||\mathbf{A}(\mu)|||\,\|\mathbf{X}(\mu)\|$, and therefore the following relative error bound:

$$\frac{\|\mathbf{e}_M(\mu)\|}{\|\mathbf{X}(\mu)\|}\leq\mathrm{cond}(\mathbf{A}(\mu))\frac{\|\mathbf{R}_M(\mu)\|}{\|\mathbf{B}\|} \tag{15}$$

with $\mathrm{cond}(\cdot)$ being the conditioning number defined by $\mathrm{cond}(\mathbf{A})=|||\mathbf{A}^{-1}|||\times|||\mathbf{A}|||$. Using classical linear algebra results, the conditioning number of a square invertible matrix $\mathbf{A}$ takes the explicit form: $\mathrm{cond}(\mathbf{A})=\sqrt{\lambda_N}/\sqrt{\lambda_1}$, with $0<\lambda_1\leq\cdots\leq\lambda_N$ the eigenvalues of the Hermitian invertible matrix $\mathbf{A}^H\mathbf{A}$. The norm of the error is therefore bounded by the norm of the residual. In practice, the error bound in (15) is known not to be sharp and very pessimistic.

3.2. Building of parametric reduced order models

Let us assume that an appropriate trial space basis $\Psi^M=[\Psi_1,\ldots,\Psi_M]\in\mathbb{C}^{N\times M}$ is already known – the building of such a basis constitutes the subject of Section 3.3. The goal of a parametric ROM is here to yield the parameter coefficients $\alpha^M(\mu)$ in (11) such that the structure–acoustic solution can be rapidly evaluated online for any parameter $\mu\in\mathcal{D}$.

The ROMs are classically obtained by performing a projection of the full model equations onto appropriate test functions $\Xi_m\in\mathbb{C}^N$, for $m=1\ldots M$. More precisely, let us introduce the low-dimensional test subspace $\mathcal{Y}_M=\mathrm{span}\{\Xi_m\}_{m=1}^M\subset\mathbb{C}^N$ as well as the low-dimensional trial subspace $\mathcal{X}_M=\mathrm{span}\{\Psi_m\}_{m=1}^M\subset\mathbb{C}^N$. The approximation of order M, $\mathbf{X}_M(\mu)\in\mathcal{X}_M$, is then defined with the weak formulation:

$$\delta\mathbf{Y}_M^H\mathbf{A}(\mu)\mathbf{X}_M(\mu)=\delta\mathbf{Y}_M^H\mathbf{B},\quad\forall\delta\mathbf{Y}_M\in\mathcal{Y}_M \tag{16}$$

For the case of a structure made of L constant properties materials, this equation can be explicitly written. More precisely, the use of Eqs. (9) and (11) yields the following system of M coupled algebraic equations:

$$\sum_{n=1}^{M}\left[\sum_{k=0}^{2(L+1)}\lambda^k(\mu)\,A_{mn}^k\right]\alpha_n(\mu)=B_m \tag{17}$$

for $m=1\ldots M$ and where the coefficients are defined by:

$$A_{mn}^k=\Xi_m^H\,\mathbf{A}^k\,\Psi_n,\quad B_m=\Xi_m^H\,\mathbf{B} \tag{18}$$

for $k=0\ldots2(L+1)$. Eq. (17) constitutes the parametric ROM. Remarks (i) and (ii) below enable us to introduce the two projections considered in this paper, respectively the Galerkin projection and the minimum residual one. Remarks (iii) and (iv) are straightforward extensions in $\mathbb{C}^N$ of classical theorems [11] on stability and *a priori* convergence established for applications in $\mathbb{R}^N$.

3.2.1. Remarks

(i) When the test space is the same as the trial one, *i.e.* $\Xi_m=\Psi_m$ for $m=1\ldots M$, Eq. (17) constitutes the Galerkin-based ROM of the discretized full model (9). In this case, the residual is orthogonal to each space function: $\Psi_m^H\mathbf{R}_M(\mu)=0$ for $m=1\ldots M$. The Galerkin-based ROM is here online-efficient [36]: the coefficients A_{mn}^k are not parameter-dependent and can be precomputed. The numerical complexity for solving online the ROM is therefore independent of the full model size.

(ii) To derive the test space for the minimum residual projection [11,44–46], let us introduce the functional $\mathcal{L}(\alpha^M)=\|\mathbf{R}_M(\mu)\|^2$. The reduced order model comes from the optimality condition of the minimization of this functional: $\alpha^M=\mathrm{argmin}_{\alpha\in\mathbb{C}^M}\mathcal{L}(\alpha)$. To achieve this goal, the variations of the functional according to the reduced coefficients have to satisfy $(\partial\mathcal{L}(\alpha)/\partial\alpha_m)\delta\alpha_m=0$ for $m=1\ldots M$. The minimum residual-based ROM comes from the explicit calculus of this optimality condition, which yields:

$$\big(\mathbf{A}(\mu)\Psi_m\big)^H\mathbf{R}_M(\mu)=0 \tag{19}$$

for $m=1\ldots M$. It clearly appears that, contrary to the Galerkin projection, the test functions $\Xi_m(\mu)=\mathbf{A}(\mu)\Psi_m$ are parameter-dependent. Nevertheless by using (8), an online-efficient version of the minimum residual-based ROM can be derived:

$$\sum_{n=1}^{M}\left[\sum_{j=0}^{2(L+1)}\sum_{k=0}^{2(L+1)}\overline{\lambda}^j(\mu)\lambda^k(\mu)\,A_{mn}^{jk}\right]\alpha_n(\mu)=\sum_{j=0}^{2(L+1)}\overline{\lambda}^j(\mu)B_m^j \tag{20}$$

for $m=1\ldots M$ and where the coefficients are defined by

$$A_{mn}^{jk}=\Psi_m^H\,\mathbf{A}^j\mathbf{A}^k\,\Psi_n,\quad B_m^j=\Psi_m^H\mathbf{A}^j\,\mathbf{B} \tag{21}$$

for $j,k=0\ldots2(L+1)$. They are therefore not parameter-dependent and can also be precomputed.

(iii) For the minimum residual projection, the reduced coefficients α are searched so that the norm of the residual is minimized; the resulting reduced order model may therefore be considered as optimal in the sense that it minimizes the $\mathbf{A}^H\mathbf{A}-$norm of the error. Furthermore the induced residual satisfies the relation

$$\begin{aligned}\|\mathbf{R}_M(\mu)\| &= \min_{\alpha\in\mathbb{C}^M}\|\mathbf{B}-\mathbf{A}(\mu)\Psi^M\alpha\|\\ &\le \|\mathbf{B}-\mathbf{A}(\mu)\Psi^M\alpha_a\|\end{aligned}$$

with α_a being an arbitrary value of α in $\mathbb{C}^M$. Then by choosing $\alpha_a=\{0,\ldots,0\}^T$, the above inequality becomes:

$$\|\mathbf{R}_M(\mu)\|\le\|\mathbf{B}-\mathbf{A}(\mu)\Psi^M\{0,\ldots,0\}^T\|=\|\mathbf{B}\|$$

The norm of the residual is therefore bounded and the reduced model may be considered as stable, in the sense that the norm of the error is itself bounded; more precisely the relation (15) reduces to

$$\|\mathbf{e}_M(\mu)\|/\|\mathbf{X}(\mu)\|\le\mathrm{cond}(\mathbf{A}(\mu))$$

(iv) Let us considered a trial space basis $\Psi^{M+1}=\left[\Psi^M,\Psi_{M+1}\right]$, so that the trial space basis Ψ^M is enriched by the space function Ψ_{M+1}. The related residual obtained with the minimum residual projection satisfies:

$$\begin{aligned}\|\mathbf{R}_{M+1}(\mu)\| &= \min_{\alpha\in\mathbb{C}^{M+1}}\|\mathbf{B}-\mathbf{A}(\mu)\Psi^{M+1}\alpha\|\\ &= \min_{(\alpha^*,\beta)\in\mathbb{C}^M\times\mathbb{C}}\left\|\mathbf{B}-\mathbf{A}(\mu)\left[\Psi^M,\Psi_{M+1}\right]\{\alpha^*,\beta\}^T\right\|\\ &\le \min_{\alpha^*\in\mathbb{C}^M}\left\|\mathbf{B}-\mathbf{A}(\mu)\left[\Psi^M,\Psi_{M+1}\right]\{\alpha^*,\beta_a\}^T\right\|\end{aligned}$$

with β_a being an arbitrary value of β in $\mathbb{C}$. Then by choosing $\beta_a=0$, the above inequality becomes:

$$\|\mathbf{R}_{M+1}(\mu)\|\le\min_{\alpha^*\in\mathbb{C}^M}\left\|\mathbf{B}-\mathbf{A}(\mu)\left[\Psi^M,\Psi_{M+1}\right]\{\alpha^*,0\}^T\right\|=\|\mathbf{R}_M(\mu)\|$$

For the minimum residual projection, the error in the $\mathbf{A}^H\mathbf{A}-$norm therefore decreases as the trial space is enriched by a new space function: $\|\mathbf{e}_{M+1}(\mu)\|_{\mathbf{A}^H\mathbf{A}}\le\|\mathbf{e}_M(\mu)\|_{\mathbf{A}^H\mathbf{A}}$. Moreover, there exists $M\le N$ for which the error is strictly decreasing, since the error is expected to be null for $M=N$ ($\mathrm{span}\{\Psi_m\}_{m=1}^N=\mathbb{C}^N$).

3.3. Offline building of an appropriate trial basis

The burning issue to build a fast, accurate and reliable parametric ROM lies in the reduced trial basis: the trial space has to be rich enough to cover most of the physics of the problem at hand, and low dimensional enough to significantly reduce the CPU time of the ROM evaluation, compared to the full model. As reminded in Section 1, established methods are available in the literature to build space bases for sub-problems of the present case of interest, and mainly for a one-dimensional parameter space (involving the frequency). Their accuracies may not be guaranteed for highly damped cases and their constructions often involve *ad hoc* processes. Meanwhile, several reduction techniques are emerging in other fields to treat generic problems with high-dimensional parameter spaces.

We address here the challenge of sampling a relatively high-dimensional parameter space to build an appropriate trial basis, by following the framework of the Reduced Basis (RB) method along with the use of a greedy algorithm [10,11]. More precisely for each new space function, we compute the exact error where the parameter $\mu\in\mathcal{D}$ maximizes the norm of the residual $\|\mathbf{R}_M(\mu)\|$, over a predetermined discrete set of parameters. This new information is then used to enrich the trial basis and to form an improved reduced order model. The use of the norm of the residual as an *a posteriori* error estimator is of course not optimal, but it remains a cheap (from the CPU time point of view) and easy to implement quantity. Finding both accurate and cheap error estimator [47,48] for the case of interest here may be a challenging topic. It constitutes a work in progress, beyond the scope of the present study.

The question of the sampling of the predetermined discrete set of parameters must also be tackled. A uniform sampling is of course prohibited for a high-dimensional parameter space: even a sparse uniform gridding in each direction would result in an extremely large number of points to evaluate the residual norm. A random sampling in $\mathcal{D}^I$ is chosen here to create the discrete set of parameters for each new space function. I is chosen sufficiently large to avoid too large regions without point in the parameter space. Moreover, a new random sampling is performed in $\mathcal{D}^I$ for each new space function, it is then expected that no important region in the parameter space will be ultimately forgotten, and that the final trial basis will be rich enough to cover most of the physics of the problem at hand. The main advantages of this sampling are its simplicity, its ease of implementation, as well as its ability to tackle relatively high dimensional parameter space (up to a five-dimensional space with a reasonable number of samples). For higher dimensional parameter spaces, other strategies should nevertheless be more appropriate. In this respect, the most elegant route to bypass the curse of dimensionality is to consider each parameter as an extra-coordinate and to perform a PGD expansion [32].

The resulting methodology is explicitly given in Algorithm 1.

Algorithm 1. Greedy algorithm for the offline computation of the trial basis.

Input: parameterized full model $\mathbf{A}(\mu)$ and $\mathbf{B}(\mu)$; full model solution $\mathbf{X}(\mu)$ on a random sampling $\mathcal{S}_I\in\mathcal{D}^I$; stopping criteria $\varepsilon<1$ and $M\ge1$

Output: Trial basis $\Psi^m=[\Psi_1,\ldots,\Psi_m]$

1: Initialization: set $\Psi^0=\emptyset$, $\alpha^0(\mu)=\emptyset$, $e_0^{\sup}=1$, $m=0$

2: **while** $(e_m^{\sup}\ge\varepsilon)$ and $(m<M)$ **do**

3: $m\leftarrow m+1$

4: Generate a random sampling of I values of the parameter $\mu\in\mathcal{D}$

$$\mathcal{S}_I=\left\{\mu^i\right\}_{i=1}^I\in\mathcal{D}^I$$

5: If $\Psi^{m-1}\neq\emptyset$, solve the ROM (Eq. (17)) for all the parameter values in $\mathcal{S}_I$

$$\alpha^{m-1}(\mu^i)\text{ for }i=1\ldots I$$

6: Identify the parameter value in $\mathcal{S}_I$ associated with the largest norm of the residual $\mathbf{R}_{m-1}(\mu)$

$$\hat{\mu}=\arg\sup_{\mu\in\mathcal{S}_I}\|\mathbf{B}(\mu)-\mathbf{A}(\mu)\Psi^{m-1}\alpha^{m-1}(\mu)\|$$

7: Evaluate the exact error, Eq. (14), at this parameter value $\hat{\mu}$

$$\mathbf{e}_{m-1}(\hat{\mu})=\mathbf{A}^{-1}(\hat{\mu})\mathbf{R}_{m-1}(\hat{\mu})$$

8: Enrich the space basis

$$\Psi_m=\frac{\mathbf{e}_{m-1}(\hat{\mu})}{\|\mathbf{e}_{m-1}(\hat{\mu})\|},\quad\Psi^m=\left[\Psi^{m-1},\Psi_m\right]$$

9: Accuracy check: compute the maximum error on the sampling $\mathcal{S}_J$:

$$e_m^{\sup} = \sup_{\mu \in \mathcal{S}_J} \| \mathbf{X}(\mu) - \Psi^m \alpha^m(\mu) \|$$

10: **end while**

3.3.1. Remarks

(i) For the random sampling $\mathcal{S}_I$, we consider in the present paper μ as a uniform random variable with values in $\mathcal{D}$. The number I of samples can – and should – be taken large in step 4, since it only involves the evaluation of I ROMs and residuals.

(ii) Either a Galerkin-based ROM or a minimum residual-based ROM can be employed at step 5 to compute the parameter coefficients. Convergence curves obtained with these two approaches are presented and commented in Section 4.

(iii) Step 7 is the most consuming part within the loop, since it has the same complexity as a full model evaluation.

(iv) The norm of the residual, or equally the $\mathbf{A}^H\mathbf{A}$–norm of the error, is used at step 6 to locate a potentially interesting place in the parameter space to perform a full model evaluation. It is not used here as a stopping criterion of the loop: the error bound (Eq. (15)) is clearly not sharp enough to this end and the link between the norms of the error and residual is too strongly case-dependent. In order to check the accuracy of the resulting ROM in step 9, it is therefore mandatory to have some full model evaluations on a predetermined random sampling $\mathcal{S}_J$. These evaluations have to be performed once and given as input of the algorithm.

4. Illustrations of the reduced models

The ROMs are illustrated here on parametric problems involving submerged viscoelastic structures. The notations are the following: *Minimum Residual RB* when a minimum residual projection is used to build the ROM and to compute the Reduced Basis in Algorithm 1 (step 4), and conversely, *Galerkin RB* when a Galerkin projection is employed. They are evaluated on the computation of the low frequency response of a submerged composite plate with a viscoelastic layer in Section 4.1, and on a more complex industrial case, the low (nearly mid) frequency response of a submerged propeller with viscoelastic patches, in Section 4.2. In both cases,

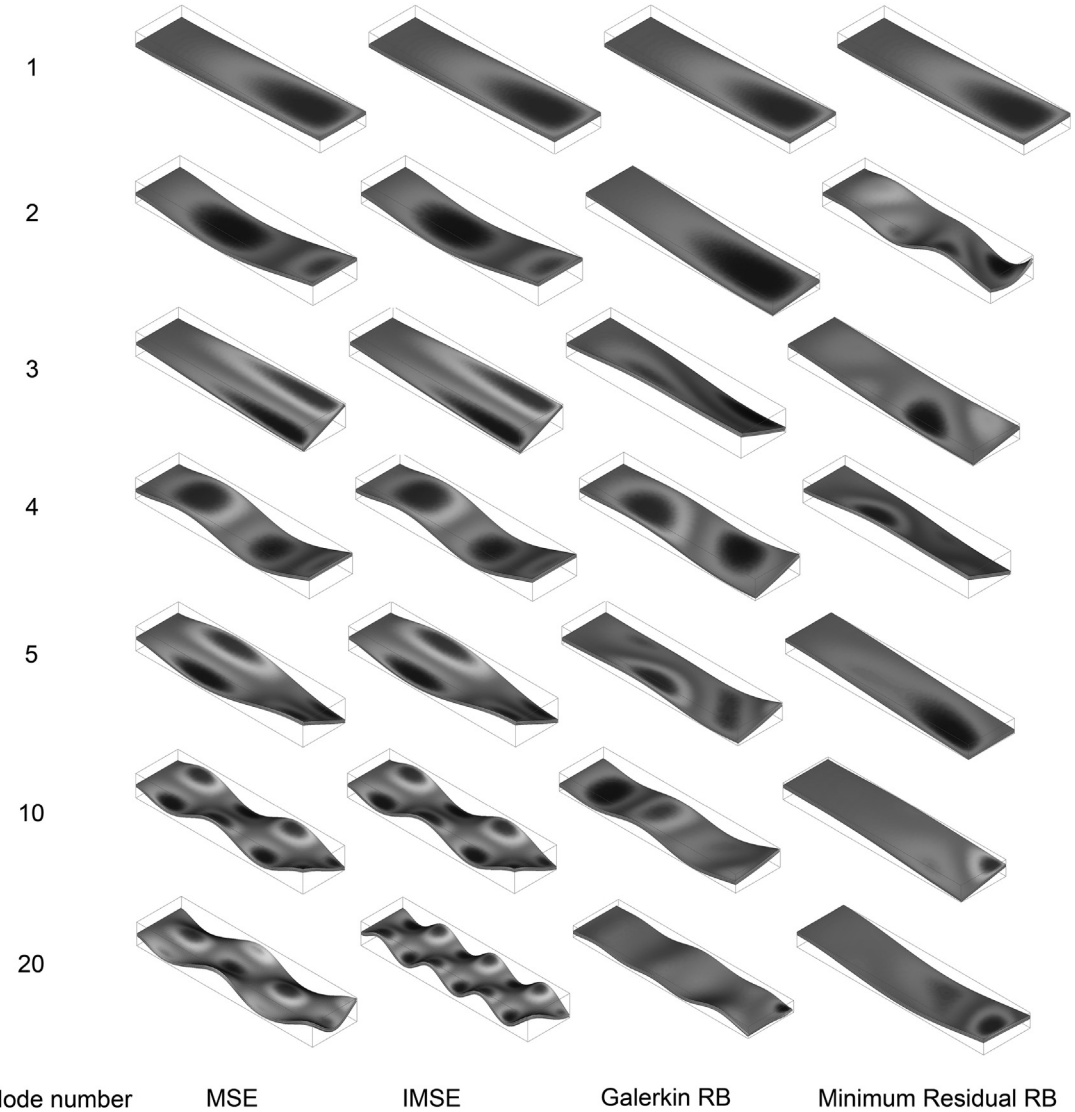

Fig. 2. Illustrations of some space functions depending on the ROMs, for the submerged composite plate case when only the frequency is varied. The real part of the deformed shape is visualized and the tones represent the pressure values on the plate surface.

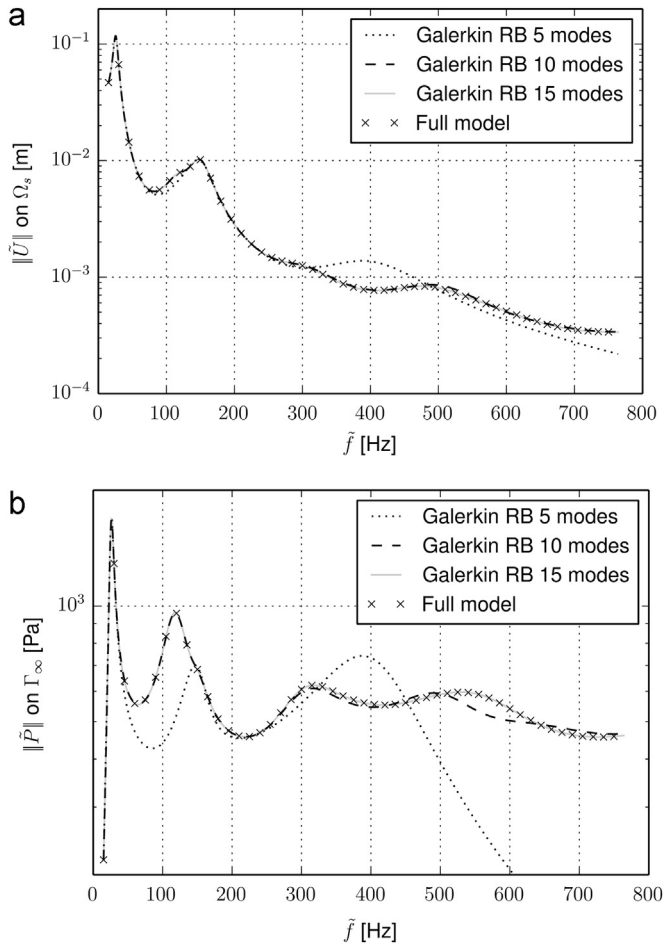

Fig. 3. Norms of the displacement and the pressure obtained with the Galerkin RB (for different values of M on a fine frequency grid) and the full model (on a coarse frequency grid) for the submerged composite plate case; (a) norms of the displacement on Ω_s, and (b) norms of the pressure on Γ_∞.

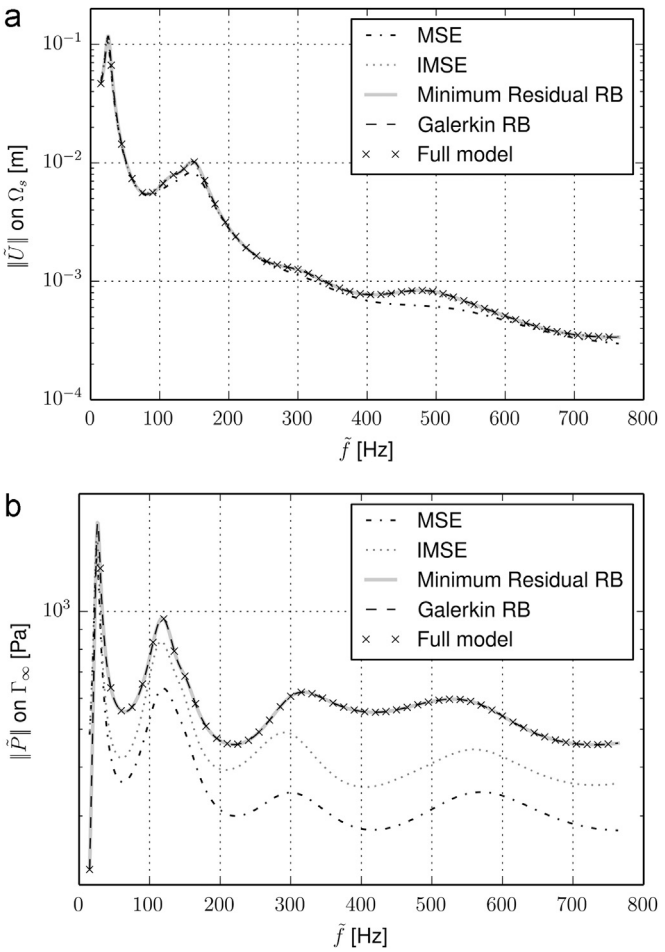

Fig. 4. Comparisons between the ROMs (with $M=25$ and on a fine frequency grid) and the full model (on a coarse frequency grid) for the submerged composite plate case; (a) norms of the displacement on Ω_s, and (b) norms of the pressure on Γ_∞.

the proposed ROMs are first evaluated on a one-dimensional parameter space – when only the frequency is varied – and compared with established approaches. The reduced models are then built and confronted on a four-dimensional parameter space, involving large variations of the material parameters.

More precisely and for a one-dimensional parameter space, comparisons are made with the MSE [14] and IMSE [15] approaches, able to tackle *in vacuo* frequency-dependent industrial problems and extended here for submerged structures. The proposed extensions are straightforward: using Eqs. (5) and (8), the trial basis with the MSE approach comes from the eigenvalue problem

$$\left[-\omega^2 \sum_{k=1}^{L+1} \rho_s^{k-1}\, \mathbf{A}^k + \sum_{k=L+2}^{2(L+1)} Re\left\{E^{k-(L+2)}(\omega_{min})\right\}\mathbf{A}^k\right]\Psi = 0 \qquad (22)$$

with ω_{min} being the minimum frequency of interest. This implies that the resulting basis contains neither the physics related to the impedance boundary condition for the acoustic domain, nor the whole complex-valued and frequency-dependent stiffness associated to the viscoelastic structures. As for the IMSE approach, the trial basis is obtained by solving iteratively (with typically three iterations), and for each mode Ψ_m, the eigenvalue problem

$$\left[-(\omega^{(i)})^2 \sum_{k=1}^{L+1} \rho_s^{k-1}\, \mathbf{A}^k + \sum_{k=L+2}^{2(L+1)} Re\left\{E^{k-(L+2)}(\omega_m^{(i-1)})\right\}\mathbf{A}^k\right]\Psi^{(i)} = 0 \qquad (23)$$

The MSE and IMSE ROMs are then obtained through a Galerkin projection of the full model (Eq. (7)) onto the corresponding computed bases.

The complexity of the proposed approaches for the offline computation of the trial basis, compared to that of the full model, is also of interest. For the full model, a large matrix system has to be inverted for each parameter value of interest, let us denote by T_{fm} the corresponding CPU time for a unique parameter value. The MSE approach requires to solve only one eigenvalue problem to obtain the space basis, which has approximately the same complexity as one full model evaluation: its CPU time is therefore T_{fm}. For the IMSE method, three eigenvalues problems are solved for each mode, this results to the CPU time $3 \times M \times T_{fm}$ if M space functions are searched. For the Minimum Residual RB and the Galerkin RB, each new space function requires to solve Eq. (14), which has exactly the same complexity as a full model. Furthermore, I ROMs have to be solved and I residual equation norms have to be evaluated, according to Algorithm 1 (steps 5 and 6) for each mode. When I is large, this may result in a noticeable CPU time, but which remains lower than a full model evaluation. It can therefore be considered that the CPU time required to compute the Reduced Bases with Algorithm 1 is approximately $M \times T_{fm}$, for the steps 1–8. As for the accuracy check, step 9, it requires the computation of J full model evaluations as input of the algorithm. The total CPU time for the computation and check of the trial basis for the RB approaches is therefore $(M+J) \times T_{fm}$. In the following, the

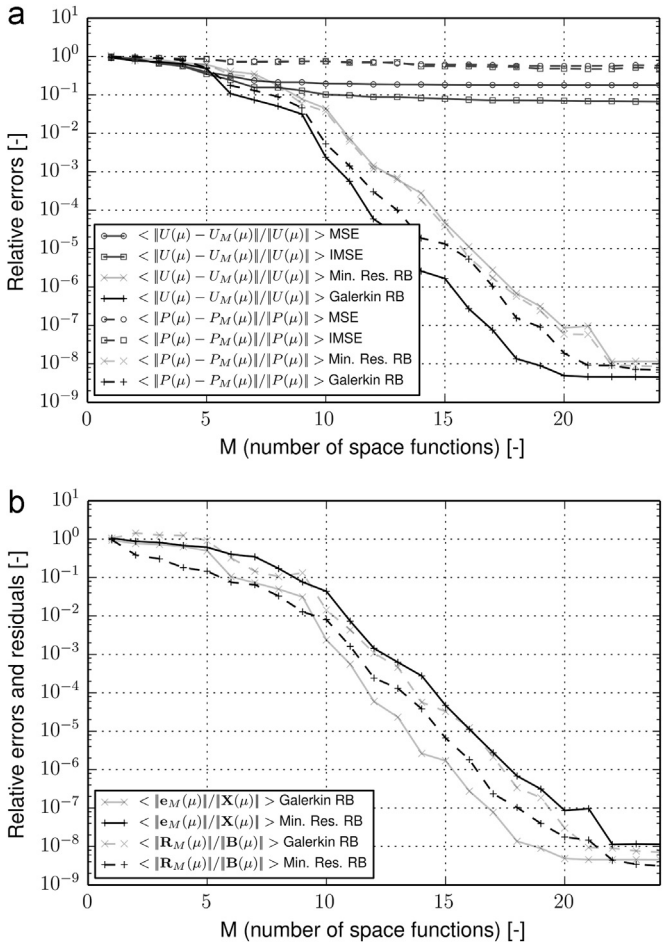

Fig. 5. Convergence of the ROMs as a function of the decomposition orders, for the submerged composite plate case, when only the frequency is varied; (a) mean of the relative error for the displacement field on Ω_s and for the pressure field on Γ_∞; (b) mean of the relative error and residual norms.

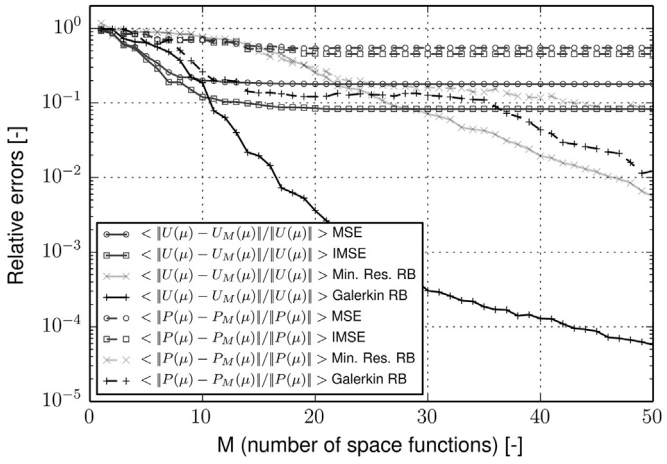

Fig. 6. Convergence of the ROMs as a function of the decomposition orders, for the submerged composite plate case, on a four-dimensional parameter space. The full model is computed on a uniform random sampling of $I=50$ values of $\mu \in (0,1)^4$. Mean of the relative error for the displacement field on Ω_s and for the pressure field on Γ_∞.

CPU time gain compared to full model evaluations will be evaluated depending on the accuracy of the resulting ROMs.

The different approaches have been implemented within the open source finite element industrial software code_aster [49] through the development of scripts written in Python language.

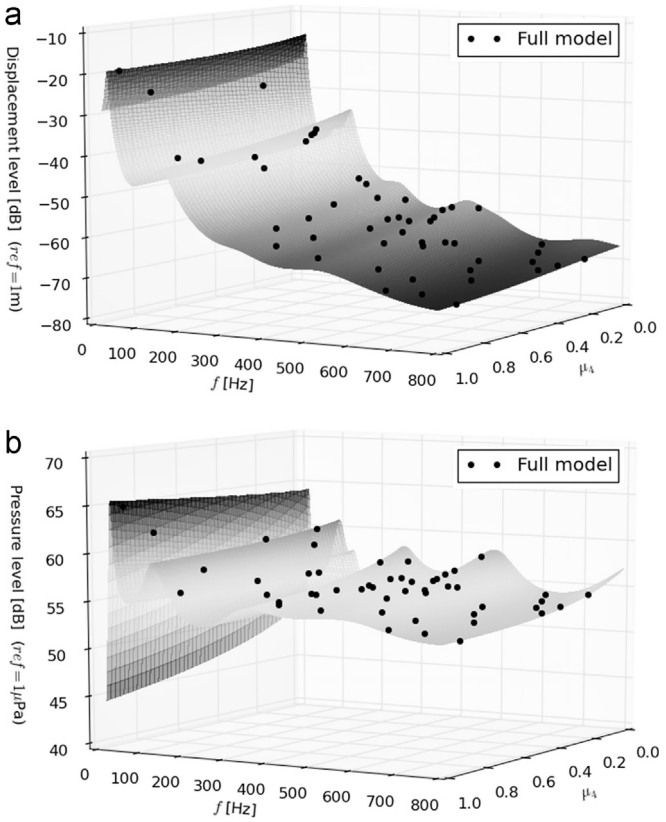

Fig. 7. Norms of the displacement and the pressure for the submerged composite plate case, obtained with the Galerkin RB for $M=50$ on the four-dimensional parameter space, according to the frequency and Young modulus of the viscoelastic material. The dots denote the corresponding values obtained with the full model, on a uniform random sampling made of $I=50$ values of $(\mu_1,\mu_4) \in (0,1)^2$; (a) norms of the displacement on Ω_s, and (b) norms of the pressure on Γ_∞.

For the two test cases, the finite element meshes are made of ten-node tetrahedral elements, generated with the pre-processing open source software Salome [50].

4.1. The submerged elastic plate with a viscoelastic layer

4.1.1. Description of the case

A submerged composite plate made of $L=2$ materials, an elastic and a viscoelastic one, is considered as illustrated in Fig. 1. The dimensional length, width and thickness of each layer are respectively given by $\tilde{L}_1 = 0.2$ m, $\tilde{L}_2 = 0.05$ m and $\tilde{e} = 0.001$ m. The elastic material is characterized by the following quantities: $\tilde{E}^1 = 1.7 \times 10^{11}$ Pa, $\nu^1 = 0.3$ and $\tilde{\rho}_s^1 = 7450$ kg m^{-3}. As for the viscoelastic layer, the density is given by $\tilde{\rho}_s^2 = 1460$ kg m^{-3} and the Poisson coefficient is considered as constant, $\nu^2 = 0.49$. Numerous viscoelastic models can be found in the literature to express the complex frequency dependent Young modulus. The fractional derivative Zener model [51,52] is chosen here since it may enable us to accurately represent the properties of the material, with a reasonable number of parameters:

$$\tilde{E}^2(\tilde{\omega}) = \frac{\tilde{E}_{v0} + \tilde{E}_{v\infty}(i\tilde{\omega}\tilde{\tau})^\alpha}{1 + (i\tilde{\omega}\tilde{\tau})^\alpha} \tag{24}$$

For the considered viscoelastic material, the values $\tilde{E}_{v0} = 6.29 \times 10^6$ Pa, $\tilde{E}_{v\infty} = 1.76 \times 10^9$ Pa, $\tilde{\tau} = 4.4 \times 10^{-7}$ s and $\alpha = 0.53$ are taken [19]. In order to account for the condition of non-reflexion of acoustic waves, the impedance $Z(\omega) = 1/(1 + \tilde{L}/(i\omega\tilde{R}_\infty))$ is applied on the spherical surface Γ_∞ of radius $\tilde{R}_\infty = 0.15$ m. The dimensional frequency band of interest is defined by $\tilde{f} \in (\tilde{f}_{min}, \tilde{f}_{max})$, with

$\tilde{f}_{min} = 15$ Hz and $\tilde{f}_{max} = 750$ Hz. From the numerical modeling point of view, the grid convergence is achieved and reliable results are obtained with 63,616 tetrahedral elements, resulting in a model containing $N = 190{,}431$ DOFs.

4.1.2. Illustrations without structural parameter variability

The proposed approaches are first compared when only the frequency is varied, *i.e.* $P=1$ and $\mu \equiv \mu_1$. Some illustrations of the space functions obtained with the MSE, IMSE, Galerkin and minimum residual Reduced Bases are presented in Fig. 2. The first mode shapes of the MSE and IMSE methods are very similar, differences can only be seen for the higher number modes. For the offline computation of the Galerkin and Minimum Residual Reduced Bases, the dimensionless frequency ω is considered as a random variable on $(\omega_{min}, \omega_{max})$, with $\omega_{min} = 2\pi\tilde{L}\tilde{f}_{min}/\tilde{c}_f$ and $\omega_{max} = 2\pi\tilde{L}\tilde{f}_{max}/\tilde{c}_f$. It is explicitly expressed as a function of the random variable $\mu \in \mathcal{D} = (0,1)$ by $\omega(\mu) = \omega_{min} + (\omega_{max} - \omega_{min})\mu$. More precisely, a uniform random sampling of $I=300$ values of $\mu \in \mathcal{D} = (0,1)$ is generated at each new space function evaluation: $\mathcal{S}_{300} = \{\mu^i\}_{i=1}^{300} \in (0,1)^{300}$. As displayed in Fig. 2, the resulting space functions for the Galerkin and Minimum Residual RB are very different from each other, illustrating that the maximum of the residual norm occurs at different parameter values.

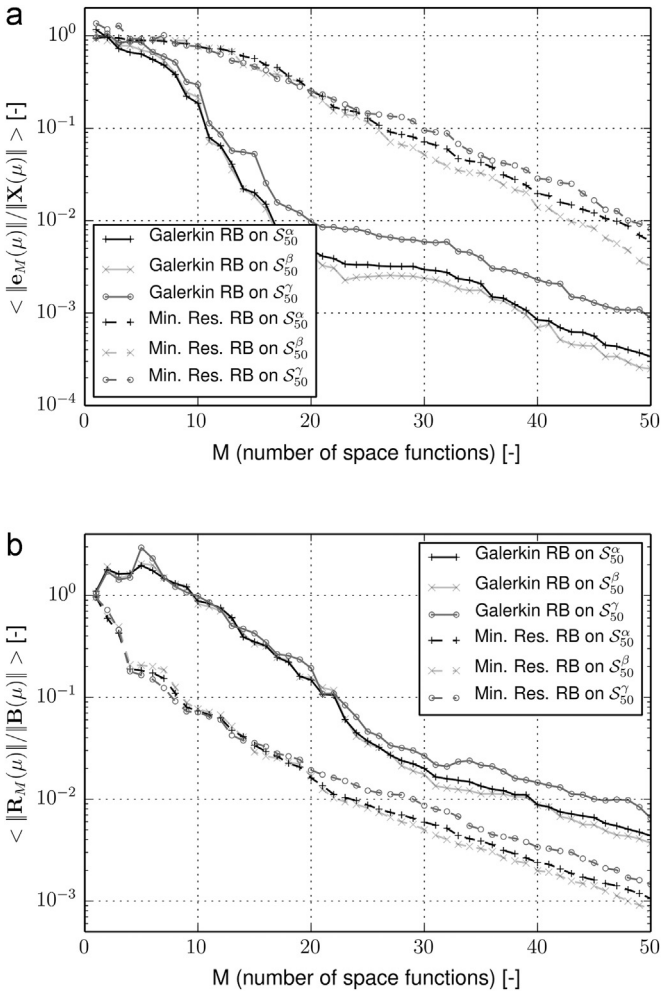

Fig. 8. Convergence of the ROMs with three different samplings on a four-dimensional parameter space, as a function of the decomposition orders, for the submerged composite plate case; (a) mean of the relative error norm, and (b) mean of the residual norm.

Once the space functions are evaluated, the reduced matrices (18) can be easily computed and the ROMs (17) straightforwardly solved. To illustrate the convergence and the accuracy of the proposed approach, the norms of the displacement and pressure obtained with the Galerkin RB for $M=5$, 10 and 15 space functions are compared to some full model evaluations in Fig. 3. Then the value $M=25$ is kept for all the considered reduced approaches and the resulting norms are displayed in Fig. 4. It clearly appears that, for the displacement field, the IMSE and the two Reduced Bases ROMs yield accurate predictions compared to the full model. Some discrepancies can only be seen for the MSE approach, reflecting that the corresponding basis is not rich enough to fully represent the highly dissipative effects of the viscoelastic layer. As far as the norm of the pressure is concerned, only the Galerkin and the Minimum Residual RBs methods are able to accurately reproduce the full model values. The MSE and IMSE strongly underestimate the pressure levels, which may be directly linked to the fact that the complex impedance boundary condition is not taken into account in the related eigenvalue problems.

To have a deeper insight on the convergence properties, the means of the relative errors between the ROMs and the full model solutions are displayed in Fig. 5(a), as functions of the decompositions order. The mean is simply defined as the average on the sampling used for the full model evaluations: $\langle f(\mu) \rangle = \sum_{j=1}^{J} f(\mu^j)/J$. Here $J=50$ full model evaluations are considered. Both Galerkin and Minimum Residual RBs methods converge to the full model solution and the Galerkin RB displays the fastest convergence properties; with both methods, 22 modes are sufficient to achieve an average error of 10^{-8} for the displacement and the pressure field. As for the MSE and IMSE approaches, they reach mean relative errors on the displacement field of respectively 20% and 7%, and more than 50% on the pressure field.

It is also fruitful to appreciate the evolution of the relative error norm along with the evolution of the residual norm, *i.e.* the relative error in the $\mathbf{A}^H\mathbf{A}-$norm. The corresponding curves are presented in Fig. 5(b). The norm of the residual obtained with the Minimum Residual RB is, as expected, inferior to the norm of the residual

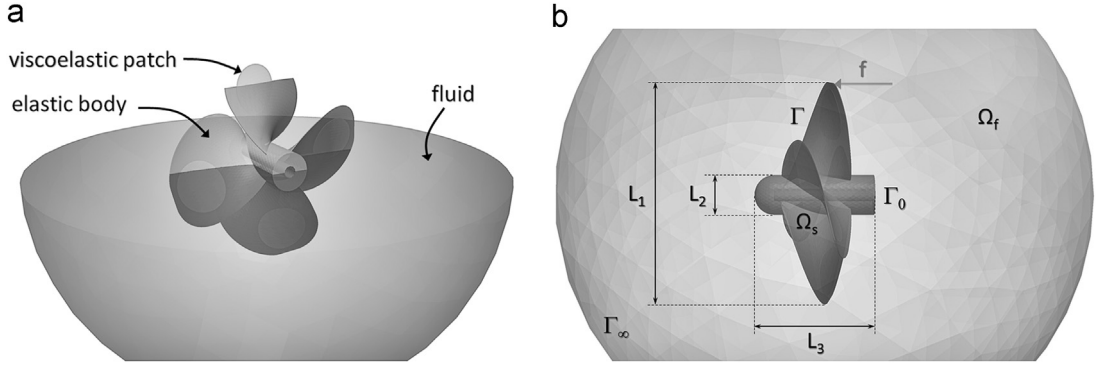

Fig. 9. Submerged propeller with embedded viscoelastic patches; (a) slices of the studied geometry, (b) mesh and notations.

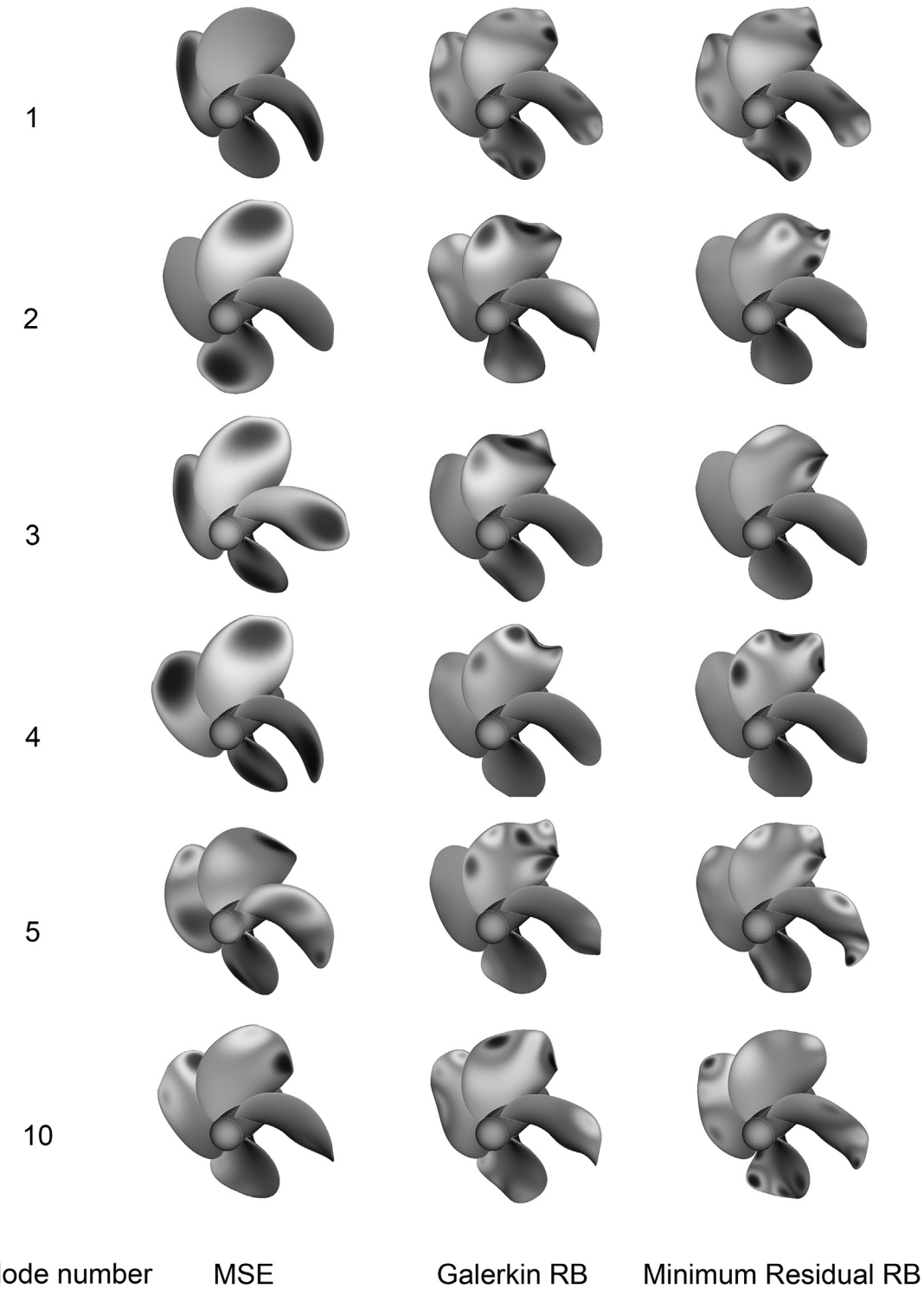

Fig. 10. Illustrations of some space functions depending on the ROMs, for the submerged propeller case, when only the frequency is varied. The real part of the deformed shape is visualized and the tones represent the pressure values on the propeller surface.

issued from the Galerkin RB. Another satisfactory point for the Minimum Residual RB is that, as mentioned in remark (iv) of Section 3.2, its residual norm monotonically decreases as the trial space is enriched. Finally, the fact that the norm of the error and the norm of the residual follow the same tendencies gives confidence to use the residual as an error estimator in the offline greedy algorithm.

As an intermediate conclusion, the MSE, which only requires a CPU time equivalent to one full model evaluation (a CPU time equal to T_{fm}), can only be used to obtain very rapidly the order of magnitude of the displacement field. The IMSE is more time consuming, with a CPU time of $25 \times 3 \times T_{fm}$, and enables us to slightly improve the displacement field evaluation. Neither the MSE nor the IMSE can however predict the pressure field, their corresponding trial bases are far from being complete enough to achieve this goal. As far as the Galerkin and Minimum Residual RBs are concerned, they can reach very accurate predictions for both the displacement and the pressure fields, with an offline CPU time of roughly $(25+50) \times T_{fm}$. The errors between the ROMs and the

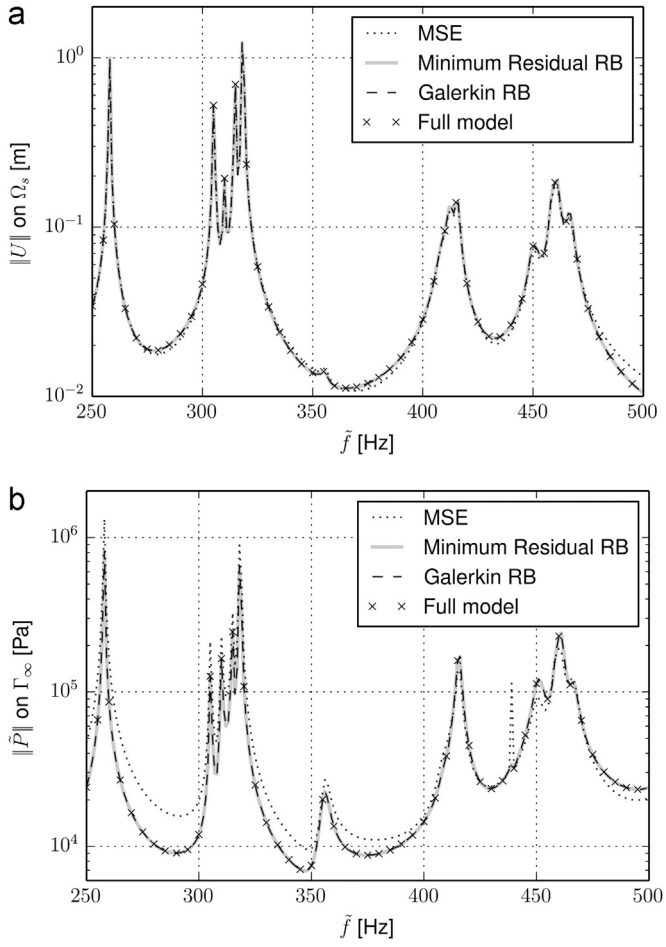

Fig. 11. Comparisons between the ROMs (with $M=35$ and on a fine frequency grid) and the full model (on a coarse frequency grid) for the submerged propeller; (a) norms of the displacement on Ω_s, and (b) norms of the pressure on Γ_∞.

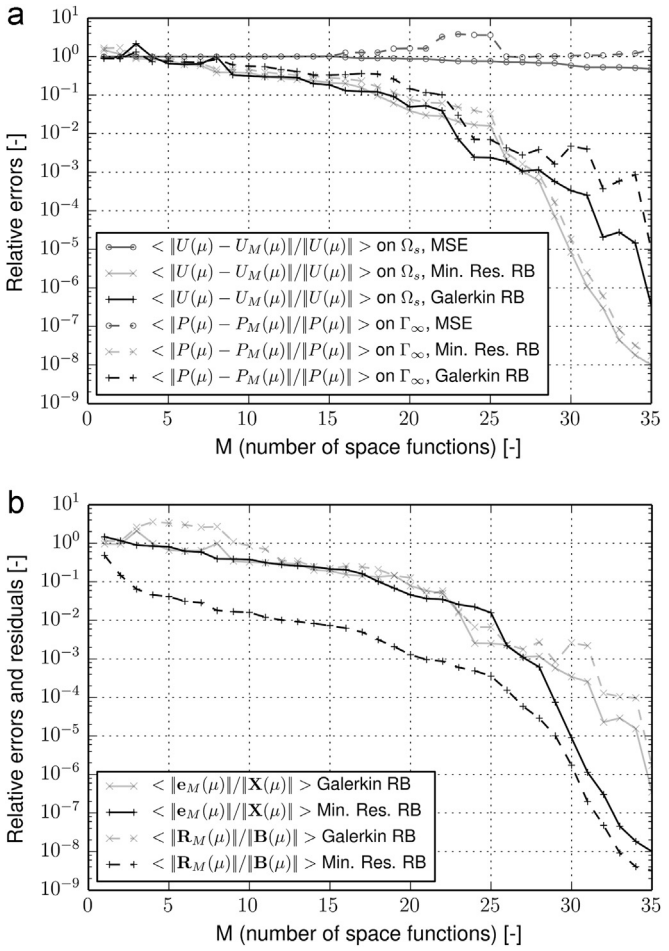

Fig. 12. Convergence of the ROMs as a function of the decomposition orders, for the submerged propeller case, when only the frequency is varied; (a) mean of the relative error on the displacement and pressure fields, and (b) mean of the relative error and residual norms.

full model have been evaluated on a coarse frequency grid made of 50 regularly spaced points in $(\tilde{f}_{min}, \tilde{f}_{max})$, therefore the total CPU time required to solve the full model is here $50 \times T_{fm}$. The Galerkin and Minimum Residual RBs can therefore be used to accurately compute structure–acoustic responses on a very fine frequency grid, with a total cost (involving the offline and online steps) equivalent to that of a full model on a coarse grid.

4.1.3. Illustrations on a four-dimensional parameter space

The Galerkin and Minimum Residual RBs are now evaluated when $P=4$ parameters are varied: the frequency, the density of the elastic material, its Young's modulus and the Young's modulus of the viscoelastic layer. They are explicitly expressed as functions of the uniform random variable $\mu \equiv \{\mu_1, \mu_2, \mu_3, \mu_4\} \in (0,1)^4$ by: $\omega(\mu) = \omega_{min} + (\omega_{max} - \omega_{min})\mu_1$, $\rho_s^1(\mu) = (1 + 0.4(\mu_2 - 0.5))\rho_s^1$, $E^1(\mu) = (1 + 0.4(\mu_3 - 0.5))E^1$ and $E^2(\mu) = (1 + (\mu_4 - 0.5))E^2$. This means that $\rho_s^1(\mu)$, $E^1(\mu)$ and $E^2(\mu)$ are uniform random variables with a variability of respectively $\pm 20\%$, $\pm 20\%$ and $\pm 50\%$ around their mean values. For the offline building of the trial bases, a sampling of $I=300$ values of $\mu \in (0,1)^4$ is generated at each new space function evaluation, $\mathcal{S}_{300} = \{\mu^i\}_{i=1}^{300} \in (0,1)^{4\times 300}$.

The convergence properties of the ROMs are illustrated as functions of the decomposition orders in Fig. 6. The mean errors for both the corresponding displacement and pressure fields are evaluated on a uniform random sampling, denoted $\mathcal{S}_{50}^{\alpha}$ and made of $I=50$ values of $\mu \in (0,1)^4$. The Galerkin and Minimum Residual RBs methods tend to the full model solution, as the order of the ROMs is increased. The convergence is nevertheless much slower than in the previous case in Fig. 5(a) and specifically for the pressure field. For instance, 50 modes enable us to reach a mean relative accuracy on the displacement field of 6×10^{-5} for the Galerkin RB, and 6×10^{-3} for the Minimum Residual RB. In order to visually illustrate the accuracy of the proposed approach, the norms of the displacement and the pressure, obtained with the Galerkin RB for $M=50$ on the four-dimensional parameter space, are compared in Fig. 7 to some full model evaluations in the two-dimensional plane $(\mu_1, \mu_4) \in (0,1)^2$.

The evolution of the relative error and residual norms are then plotted in Fig. 8, as functions of the decomposition orders and on two other samplings: $\mathcal{S}_{50}^{\beta}$ (consisting of 50 regularly spaced frequencies in $(\omega_{min}, \omega_{max})$ with the other parameters fixed at median values) and $\mathcal{S}_{50}^{\gamma}$ (made of 50 regularly spaced frequencies in $(\omega_{min}, \omega_{max})$, with the other parameters fixed at boundaries of the considered space: $\rho_{s1}(\mu) = 1.2 \times \rho_{s1}$, $E_1(\mu) = 0.8 \times E_1$ and $E_2(\mu) = 0.5 \times E_2$). It can be seen in Fig. 8 (a) that, on the three considered samplings, the Galerkin RB displays faster convergence curves for the relative error norms than the Minimum Residual RB; an opposite behavior is observed for the evolution of the residual norms in Fig. 8(b). For the Minimum Residual RB, a monotonic decrease of the residual norm can be clearly seen as the trial space is enriched. Finally, the errors have the same order of magnitude on the three samplings; the most accurate predictions occur at the

center of the parameter space (on $\mathcal{S}_{50}^{\beta}$), and conversely, the least accurate ones happen at the boundaries (on $\mathcal{S}_{50}^{\gamma}$).

The proposed Galerkin and Minimum Residual RBs therefore enable us to build relatively accurate ROMs on a whole multi-dimensional parameter space. If a structure–acoustic response is expected on a very coarse regular gridding of the parameter space, made of 20 points per dimension for instance, then the total CPU time required to solve the full model would be $20^4 \times T_{fm}$. Here a reasonably accurate prediction of the vibro-acoustic response can be achieved with a trial subspace of dimension 50, which implies an offline CPU time of $(50+50) \times T_{fm}$ for the reduced basis, including an accuracy check on $J=50$ samples. The induced CPU time gain is therefore around $20^4/100 = 1600$. Much larger gains can of course occur for applications which require the response evaluations on finer grids, as in sensitivity analysis and propagation of uncertainties studies.

4.2. Submerged propeller with viscoelastic patches

4.2.1. Description of the case

The response of a submerged propeller is of interest in this section, in order to evaluate the proposed approaches on a large-scale problem with a relatively high modal density. It is made of $L=2$ materials: an elastic core and four embedded viscoelastic patches, as shown in Fig. 9. The dimensional lengths are given by $\tilde{L}_1 = 1.8$ m, $\tilde{L}_2 = 0.33$ m, $\tilde{L}_3 = 1.0$ m and the thickness of the patches is $\tilde{e} = 0.003$ m. The impedance boundary condition is imposed on a spherical surface of radius $\tilde{R}_{\infty} = 2.0$ m. The properties of the elastic and viscoelastic materials are exactly the same as those in Section 4.1.1. The dimensional frequency band of interest is here at the transition between the low and mid frequencies for the propeller: $\tilde{f} \in (\tilde{f}_{min}, \tilde{f}_{max})$ with $\tilde{f}_{min} = 250$ Hz and $\tilde{f}_{max} = 500$ Hz. Reliable results are presented on a mesh made of 265,549 tetrahedral elements, involving $N=826{,}746$ DOFs. This case has therefore the complexity of an industrial problem.

4.2.2. Illustrations without structural parameter variability

The space functions obtained with the MSE, Galerkin and Minimum Residual Reduced Bases are illustrated in Fig. 10. For the Galerkin and Minimum Residual RBs, the dimensionless frequency $\omega(\mu)$ is seen as a random variable and a uniform random sampling of $I=300$ values of $\mu \in \mathcal{D} = (0,1)$ is generated at each new space function evaluation.

The ROMs are then solved on a fine frequency grid with 35 space functions and the resulting displacement and pressure norms are presented in Fig. 11. No differences can be seen between the Galerkin RB, the Minimum Residual RB and the full model. The MSE displays some noticeable discrepancies, in particular for the pressure. The tendencies are reproduced but the pressure levels appear mostly to be overestimated with the MSE.

The convergence properties of the ROMs are presented in Fig. 12 as functions of the decomposition order. A poor convergence can be observed for the errors obtained with the MSE in Fig. 12(a): mean relative errors of 50% and 150% are obtained for respectively the displacement and pressure norms, with 35 modes. On the contrary, the Galerkin and Minimum Residual RBs display very fast convergence properties, the most efficient being obtained this time with the Minimum Residual RB. The evolutions of the whole relative error and residual norms are displayed in Fig. 12(b). More regular curves are observed for the Minimum Residual RB and as expected, the resulting residual norm is monotonically decreasing and inferior to the residual norm issued from the Galerkin RB. The intermediate conclusion formulated in Section 4.1.2 also holds on this industrial case.

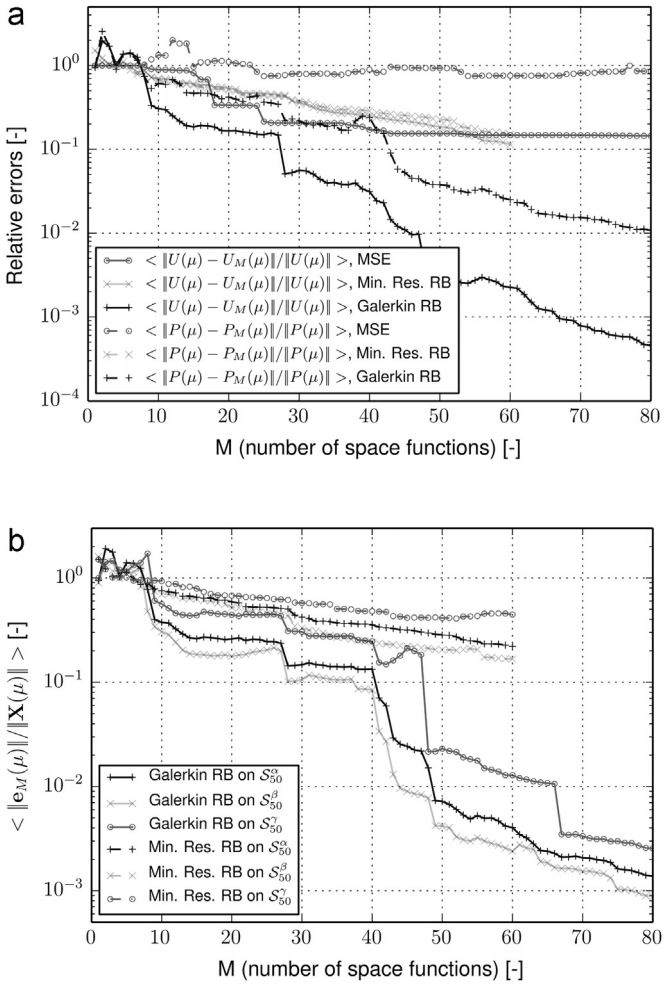

Fig. 13. Convergence of the ROMs as a function of the decomposition orders, for the submerged propeller case, on a four-dimensional parameter space; (a) mean of the relative error for the displacement and pressure fields, on a uniform random sampling of $I=50$ values of $\mu \in (0,1)^4$; (b) mean of the relative error with three different samplings.

4.2.3. Illustrations on a four-dimensional parameter space

The Galerkin and Minimum Residual RBs are now evaluated when $P=4$ parameters are varied. For the offline computation of the reduced bases, the parameters are considered as functions of $\mu \in (0,1)^4$, with the same variability as that used for the composite plate. A sampling of $I=300$ values of μ is generated at each new space function evaluation.

The mean errors for the displacement and pressure fields, obtained with the resulting ROMs on a uniform random sampling, are plotted in Fig. 13(a), as functions of the decomposition orders. The sampling denoted $\mathcal{S}_{50}^{\alpha}$ is made of $I=50$ values of $\mu \in (0,1)^4$. Due to the relatively high modal density, the convergence of the Galerkin and Minimum Residual RBs is slower than in the previous case. For the Galerkin RB approach, the achieved accuracy may however be considered as reasonable, from the point of view of the reduced order modeling: mean errors of $5 \cdot 10^{-4}$ for the displacement and 10^{-2} for the pressure are reached with $M=80$ space functions. As for the Minimum Residual RB, the convergence rate is here rather poor and mean relative errors around 10–20% are only achieved with $M=60$ space functions. Note also that larger M are not considered for the Minimum Residual RB due to the resulting ill-conditioned reduced matrices to invert. The relative error norms for the two proposed ROMs are illustrated in Fig. 13(b) on the

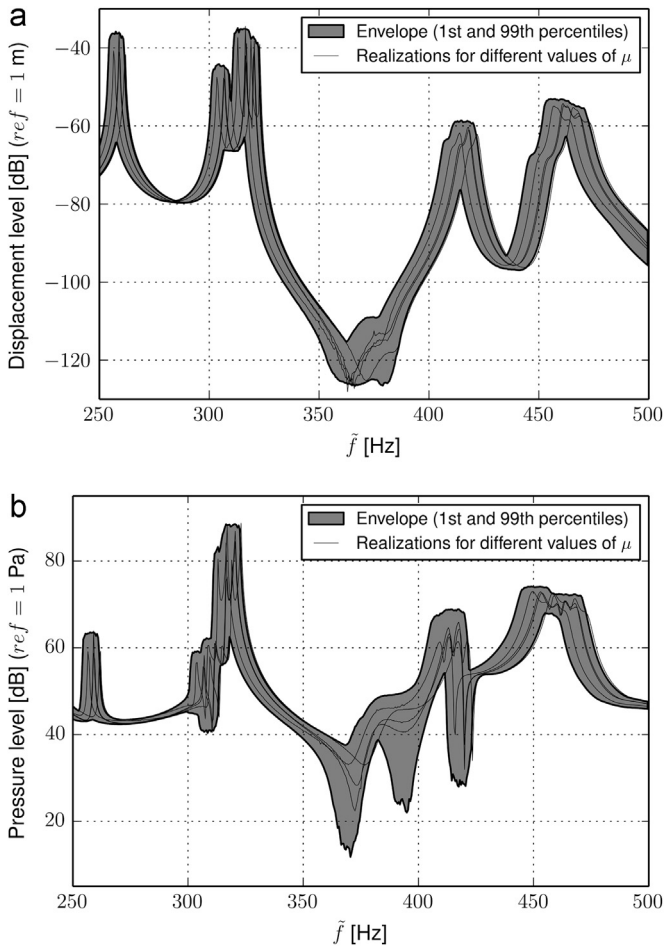

Fig. 14. Envelope of the frequency response for the submerged propeller case obtained with the Galerkin RB approach. The frequency is regularly discretized with 500 points in (250, 500) Hz. The three material parameters, $\rho_s^1(\mu)$, $E^1(\mu)$ and $E^2(\mu)$ are considered as uniform random variables with a variability of respectively 2%, 2% and 40% around their mean values; the envelopes of the response are computed on a sampling of $I=2000$ values of the parameters, for each frequency. (a) Displacement level on a point located at the end of a blade, and (b) pressure level at a point on Γ_∞.

samplings $\mathcal{S}_{50}^{\alpha}$, $\mathcal{S}_{50}^{\beta}$ and $\mathcal{S}_{50}^{\gamma}$ already introduced in Section 4.1.3. On these three samplings, the Galerkin RB displays much better performance than the Minimum Residual RB. As remarked for the plate case, the predictions appear to be slightly more accurate at the center of the parameter space than at the boundaries.

To illustrate a possible application of the proposed ROMs, envelopes of the displacement and pressure frequency responses obtained with the Galerkin RB approach are displayed in Fig. 14. The frequency is regularly discretized with 500 points in (250, 500) Hz. The three material parameters, $\rho_s^1(\mu)$, $E^1(\mu)$ and $E^2(\mu)$ are here considered as uniform random variables with a variability of respectively 2%, 2% and 40% around their mean values, which lies in the validity domain of the Galerkin RB built on a larger parameter space. The envelopes of the response are computed on a sampling of $I=2000$ values of the parameters for each frequency, 10^6 ROM evaluations are therefore done. The CPU time gain compared to full model evaluations is here $10^6/(80+50)\approx 7000$, since the Galerkin RB based ROM involves 80 space functions and the accuracy check is made of $J=50$ samples. A unique full model evaluation is in this case rather expensive (around 2 h on a standard workstation with 12 cores), therefore such envelopes obtained with 10^6 evaluations is clearly not reachable without ROM strategies.

5. Conclusion

Low dimensional space-parameter separated representations are developed and evaluated for the reduced order modeling of parametric viscoelastic structure–acoustic interaction problems. A symmetrical formulation, chosen to model the structure–acoustic interaction problem, is first turned into a parameterized matrix system, constituting the full model of reference. For the reduced order modeling, a monolithic separated representation is adopted and both Galerkin and minimum residual projections are performed. The challenge of sampling a relatively high-dimensional parameter space to build the trial basis is addressed, by following the framework of the Reduced Basis method and by using a dedicated greedy algorithm. For each new space function, the exact error where the parameter maximizes the error estimator – over a uniform random predetermined sampling – is computed and used to enrich the trial basis.

The accuracy of the resulting ROMs is evaluated on two test cases: a submerged viscoelastic composite plate corresponding to a low modal density situation, and a submerged propeller with viscoelastic patches of industrial complexity and higher modal density. The proposed ROMs are compared to established methods conceived to tackle *in vacuo* viscoelastic problems, and extended here for studies involving submerged structures. On a one-dimensional parameter space (when only the frequency is varied), it is numerically shown that the ROMs can reach much higher accuracies than the existing approaches, for both the displacement and the pressure fields. On a four-dimensional parameter space, reasonably accurate predictions are achieved with the Galerkin RB based ROM. The CPU time gain compared to the full model evaluations is of several orders of magnitude, depending on the desired applications, opening the way to new design strategies in the naval industry.

Future works may include the search of a more sophisticated error estimator than the residual norm, in order to both improve the convergence properties of the ROMs and yield a reliable stopping criterion for the greedy algorithm. For industrial purpose and to simplify the mesh complexity, the development and evaluation of the proposed approach starting from a FEM/BEM discretized formulation may furthermore be a fruitful extension of the work. Alternative algorithms to build the separated space-parameter representation could also be conceived; the Generalized Spectral Decomposition is a good candidate and constitutes a work-in-progress.

References

[1] P. Holmes, J.L. Lumley, G. Berkooz, C.W. Rowley, Turbulence, Coherent Structures, Dynamical Systems and Symmetry, 2nd edition, Cambridge University Press, Cambridge, 2012.
[2] K. Willcox, J. Peraire, Balanced model reduction via the Proper Orthogonal Decomposition, AIAA J. 40 (2002) 2323–2330, http://dx.doi.org/10.2514/6.2001-2611.
[3] D. Ryckelynck, A priori hyperreduction method: an adaptive approach, J. Comput. Phys. 202 (1) (2005) 346–366, http://dx.doi.org/10.1016/j.jcp.2004.07.015.
[4] C. Allery, A. Hamdouni, D. Ryckelynck, N. Verdon, A priori reduction method for solving the two-dimensional Burgers equations, Appl. Math. Comput. 217 (15) (2011) 6671–6679, http://dx.doi.org/10.1016/j.amc.2011.01.065.
[5] A. Ammar, B. Mokdad, F. Chinesta, R. Keunings, A new family of solvers for some classes of multidimensional partial differential equations encountered in kinetic theory modeling of complex fluids, J. Non-Newton. Fluid Mech. 139 (3) (2006) 153–176, http://dx.doi.org/10.1016/j.jnnfm.2006.07.007.
[6] A. Nouy, A priori model reduction through Proper Generalized Decomposition for solving time-dependent partial differential equations, Comput. Methods Appl. Mech. Eng. 199 (23–24) (2010) 1603–1626, http://dx.doi.org/10.1016/j.cma.2010.01.009.
[7] A. Dumon, C. Allery, A. Ammar, Proper general decomposition (PGD) for the resolution of Navier–Stokes equations, J. Comput. Phys. 230 (4) (2011) 1387–1407, http://dx.doi.org/10.1016/j.jcp.2010.11.010.

[8] C. Leblond, C. Allery, A priori space-time separated representation for the reduced order modeling of low Reynolds number flows, Comput. Methods Appl. Mech. Eng. 274 (0) (2014) 264–288, http://dx.doi.org/10.1016/j.cma.2014.02.010.
[9] A. Barbarulo, P. Ladevze, H. Riou, L. Kovalevsky, Proper Generalized Decomposition applied to linear acoustic: a new tool for broad band calculation, J. Sound Vib. 333 (2014) 2422–2431, http://dx.doi.org/10.1016/j.jsv.2014.01.014.
[10] M.A. Grepl, A.T. Patera, A posteriori error bounds for reduced-basis approximations of parametrized parabolic partial differential equations, ESAIM: Math. Model. Numer. Anal. 39 (2005) 157–181, http://dx.doi.org/10.1051/m2an:2005006.
[11] T. Bui-Thanh, K. Willcox, O. Ghattas, Model reduction for large-scale systems with high-dimensional parametric input space, SIAM J. Sci. Comput. 30 (6) (2008) 3270–3288, http://dx.doi.org/10.1137/070694855.
[12] A. Placzek, D.-M. Tran, R. Ohayon, Hybrid proper orthogonal decomposition formulation for linear structural dynamics, J. Sound Vib. 318 (4–5) (2008) 943–964, http://dx.doi.org/10.1016/j.jsv.2008.05.015.
[13] F.A. Lulf, D.-M. Tran, R. Ohayon, Reduced bases for nonlinear structural dynamic systems: a comparative study, J. Sound Vib. 332 (15) (2013) 3897–3921, http://dx.doi.org/10.1016/j.jsv.2013.02.014.
[14] C. Johnson, D. Kienholz, Finite element prediction of damping in structures with constrained viscoelastic layers, AIAA J. 20 (1982) 1284–1290, http://dx.doi.org/10.2514/3.51190.
[15] B.-G. Hu, M. Dokaishi, W. Mansour, A modified MSE method for viscoelastic systems: a weighted stiffness matrix approach, Trans. ASME 117 (1995) 226–231, http://dx.doi.org/10.1115/1.2873923.
[16] R.M. Lin, M.K. Lim, Complex eigensensitivity based characterization of structures with viscoelastic damping, J. Acoust. Soc. Am. 100 (5) (1996) 3182–3191, http://dx.doi.org/10.1121/1.417202.
[17] L. Duigou, E.M. Daya, M. Potier-Ferry, Iterative algorithms for non-linear eigenvalue problems. Application to vibrations of viscoelastic shells, Comput. Methods Appl. Mech. Eng. 192 (11–12) (2003) 1323–1335, http://dx.doi.org/10.1016/S0045-7825(02)00641-2.
[18] E. Balmès, Parametric families of reduced finite element models. Theory and applications, Mech. Syst. Signal Process. 10 (4) (1996) 381–394, http://dx.doi.org/10.1006/mssp.1996.0027.
[19] L. Rouleau, Modélisation vibro-acoustique de structures sandwich munies de matériaux viscoélastiques (Ph.D. thesis), Conservatoire National des Arts et Métiers, 2013.
[20] C. Germoso, A. Fraile, E. Alarcon, J.V. Aguado, F. Chinesta, From standard to fractional structural visco-elastodynamics: application to seismic site response, Phys. Chem. Earth, Parts A/B/C 2016, http://dx.doi.org/10.1016/j.pce.2016.01.005 (in press), ISSN 1474-7065.
[21] J. Aguado, A. Huerta, F. Chinesta, E. Cueto, Real-time monitoring of thermal processes by reduced-order modeling, Int. J. Numer. Methods Eng. 102 (2015) 991–1017.
[22] C. Guermoso, J. Aguado, A. Fraile, E. Alarcon, F. Chinesta, Efficient PGD-based dynamic calculation of non-linear soil behavior, C. R. Méc. 344 (2016) 24–41.
[23] R. Ohayon, Reduced symmetric models for modal analysis of internal structural-acoustic and hydroelastic-sloshing systems, Comput. Methods Appl. Mech. Eng. 190 (24–25) (2001) 3009–3019, http://dx.doi.org/10.1016/S0045-7825(00)00379-0.
[24] R. Ohayon, C. Soize, Advanced computational dissipative structural acoustics and fluid–structure interaction in low- and medium-frequency domains. Reduced-order models and uncertainty quantification, Int. J. Aeronaut. Space Sci. 13 (2012) 14–40, http://dx.doi.org/10.5139/IJASS.2012.13.2.127.
[25] C. Leblond, J. Sigrist, B. Auvity, H. Peerhossaini, A semi-analytical approach to the study of an elastic circular cylinder confined in a cylindrical fluid domain subjected to small-amplitude transient motions, J. Fluids Struct. 25 (1) (2009) 134–154, http://dx.doi.org/10.1016/j.jfluidstructs.2008.04.004.
[26] C. Leblond, J.-F. Sigrist, A versatile approach to the study of the transient response of a submerged thin shell, J. Sound Vib. 329 (1) (2010) 56–71, http://dx.doi.org/10.1016/j.jsv.2009.08.024.
[27] S. Assaf, M. Guerich, P. Cuvelier, Vibration and acoustic response of damped sandwich plates immersed in a light or heavy fluid, Comput. Struct. 88 (13–14) (2010) 870–878, http://dx.doi.org/10.1016/j.compstruc.2010.04.006.
[28] T. Lieu, C. Farhat, M. Lesoinne, Reduced-order fluid/structure modeling of complete aircraft configuration, Comput. Methods Appl. Mech. Eng. 195 (2006) 5730–5742.
[29] D. Amsallem, C. Farhat, Interpolation method for adapting reduced-order models and application to aeroelasticity, AIAA J. 46 (2008) 1803.
[30] E. Prulière, F. Chinesta, A. Ammar, On the deterministic solution of multidimensional parametric models using the Proper Generalized Decomposition, Math. Comput. Simul. 81 (4) (2010) 791–810, http://dx.doi.org/10.1016/j.matcom.2010.07.015.
[31] M. Chevreuil, A. Nouy, Model order reduction based on proper generalized decomposition for the propagation of uncertainties in structural dynamics, Int. J. Numer. Methods Eng. 89 (2) (2012) 241–268, http://dx.doi.org/10.1002/nme.3249.
[32] F. Chinesta, A. Leygue, F. Bordeu, J. Aguado, E. Cueto, D. Gonzalez, I. Alfaro, A. Ammar, A. Huerta, PGD-based computational vademecum for efficient design, optimization and control, Arch. Comput. Methods Eng. 20 (1) (2013) 31–59, http://dx.doi.org/10.1007/s11831-013-9080-x.
[33] M. Chevreuil, C. Leblond, A. Nouy, J. Sigrist, Model reduction method for the computation of a low frequency random vibro-acoustic response, in: 11th World Congress on Computational Mechanics (WCCM XI), Barcelona, Spain, 20–25 July, 2014.
[34] M. Chevreuil, Y. Tampango, C. Leblond, A. Nouy, J. Sigrist, Sampling-based model reduction method for the computation of low-frequency random vibro-acoustic response, in: International Conference on Uncertainty Quantification in Computational Sciences and Engineering, Crete Island, 25–27 May, 2015.
[35] S. Boyaval, C. LeBris, T. Lelièvre, Y. Maday, N. Nguyen, A. Patera, Reduced basis techniques for stochastic problems, Arch. Comput. Methods Eng. 17 (4) (2010) 435–454, http://dx.doi.org/10.1007/s11831-010-9056-z.
[36] F. Casenave, A. Ern, T. Lelièvre, A nonintrusive reduced basis method applied to aeroacoustic simulations, Adv. Comput. Math. (2014) 1–26, http://dx.doi.org/10.1007/s10444-014-9365-0.
[37] H. Morand, R. Ohayon, Fluid Structure Interaction: Applied Numerical Methods, Wiley, New York, 1995.
[38] J.-F. Sigrist, Fluid–Structure Interaction: An Introduction to Finite Element Coupling, Wiley, United Kingdom, 2015.
[39] A. Bayliss, M. Gunzburger, E. Turkel, Boundary conditions for the numerical solution of elliptic equations in exterior regions, SIAM J. Appl. Math. 42 (2) (1982) 430–451, http://dx.doi.org/10.1137/0142032.
[40] I. Harari, R. Djellouli, Analytical study of the effect of wave number on the performance of local absorbing boundary conditions for acoustic scattering, Appl. Numer. Math. 50 (1) (2004) 15–47, http://dx.doi.org/10.1016/j.apnum.2003.11.007.
[41] D. Leray, Y. Goth, Acoustic calculation with the free solver code_aster, in: Proceedings of International Compressor Engineering Conference Paper 2133.
[42] M. Barrault, Y. Maday, N.C. Nguyen, A.T. Patera, An empirical interpolation method: application to efficient reduced-basis discretization of partial differential equations, C. R. l´Acad. Sci. – Ser. 339 (2004) 667–672.
[43] F. Cazenave, Méthodes de réduction de modèles appliquées à des problèmes d´aéroacoustique résolus par équations intégrales (Ph.D. thesis), Université Paris-Est, 2013.
[44] T. Bui-Thanh, K. Willcox, O. Ghattas, B. van Bloemen Waanders, Goal-oriented, model-constrained optimization for reduction of large-scale systems, J. Comput. Phys. 224 (2) (2007) 880–896, http://dx.doi.org/10.1016/j.jcp.2006.10.026.
[45] C. Leblond, C. Allery, C. Inard, An optimal projection method for the reduced-order modeling of incompressible flows, Comput. Methods Appl. Mech. Eng. 200 (33–36) (2011) 2507–2527, http://dx.doi.org/10.1016/j.cma.2011.04.020.
[46] A. Tallet, C. Allery, C. Leblond, E. Liberge, A minimum residual projection to build coupled velocity-pressure POD-ROM for incompressible Navier–Stokes equations, Commun. Nonlinear Sci. Numer. Simul. 22 (2015) 909–932, http://dx.doi.org/10.1016/j.cnsns.2014.09.009.
[47] D. Huynh, G. Rozza, S. Sen, A. Patera, A successive constraint linear optimization method for lower bounds of parametric coercivity and inf–sup stability constants, C. R. l´Acad. Sci. – Ser. I 345 (2007) 473–478.
[48] D. Huynh, D. Knezevic, Y. Chen, J. Hesthaven, A. Patera, A natural-norm successive constraint method for inf–sup lower bounds, Comput. Methods Appl. Mech. Eng. 199 (2010) 1963–1975.
[49] Code_Aster Open Source – General FEA Software, EDF R&D, URL ⟨www.code-aster.org⟩.
[50] Salome – The Open Source Integration Platform for Numerical Simulation, URL ⟨www.salome-platform.org⟩.
[51] A.C. Galucio, J.-F. Deu, R. Ohayon, Finite element formulation of viscoelastic sandwich beams using fractional derivative operators, Comput. Mech. 33 (4) (2004) 282–291, http://dx.doi.org/10.1007/s00466-003-0529-x.
[52] L. Rouleau, J.-F. Deu, A. Legay, J.-F. Sigrist, Vibro-acoustic study of a viscoelastic sandwich ring immersed in water, J. Sound Vib. 331 (3) (2012) 522–539, http://dx.doi.org/10.1016/j.jsv.2011.10.004.